AFIT/GA/ENY/91D-5

NAVIGATION OF A SATELLITE CLUSTER WITH REALISTIC DYNAMICS

THESIS

J. Timothy Middendorf

AFIT/GA/ENY/91D-5

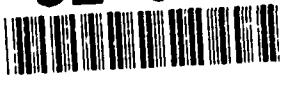

AFIT/GA/ENY/91D-5

NAVIGATION OF A SATELLITE CLUSTER WITH REALISTIC DYNAMICS

THESIS

Presented to the Faculty of the School of Engineering

of the Air Force Institute of Technology

Air University

In Partial Fulfillment of the

Requirements for the Degree of

Master of Science in Astronautical Engineering

J. Timothy Middendorf, B.S.

Captain, USAF

December, 1991

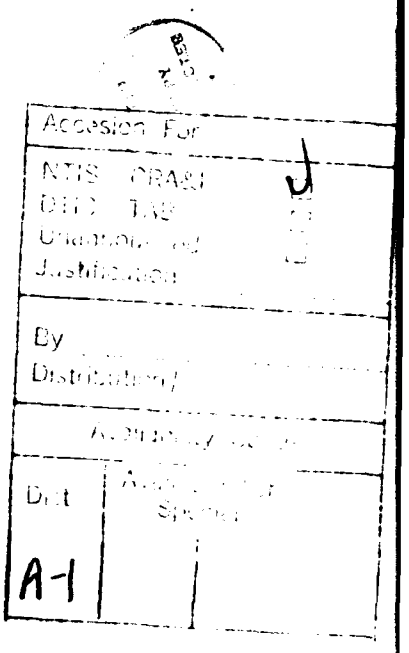

Preface

> Finally, as all our observations, on account of the imperfection of the instruments and of the senses, are only approximations to the truth, an orbit based only on the six absolutely necessary data may be still liable to considerable errors. In order to diminish these as much as possible, and thus to reach the greatest precision attainable, no other method will be given except to accumulate the greatest number of the most perfect observations, and to adjust the elements, not so as to satisfy this or that set of observations with absolute exactness, but so as to agree with all in the best possible manner. [1:51]

Carl Friedrich Gauss, quoted above, was the founder of estimation theory. He laid the ground work for all modern estimation. Today, optimal estimation has been claimed by the Kalman filter. This study used the iterated, extended Kalman filter to investigate the performance of an on-board filter used to estimate the relative positions of a cluster of satellites navigating in the presence of *real* dynamics. But it wasn't just the Kalman filter that allowed this research to be possible.

Thank you to all who aided me in this endeavor. I wish to specifically thank Dr. William E. Wiesel, my thesis advisor, for his patience, guidance and good humor during this research. Additionally, I want to thank Dr. Wiesel and Dr. Rodney Bain for the enjoyment I received from their astrodynamics classes. Also I thank Dr. Peter Maybeck for his time and counsel. I wish to thank Capt John Gustafson for his advice.

My unending love and thanks are due my wife Joan and son Stephen for their patience, understanding and support for these past months. Finally, I thank our Lord for the endurance to see this through. I pray in some way this serves His purpose, otherwise it will have been for nothing.

J. Timothy Middendorf

Table of Contents

List of Figures

List of Symbols

a	Semi-major axis
e	Eccentricity
i	Inclination
ω	Argument of Perigee
Ω	Right Ascension of the Ascending Node
η	Mean Motion
η_K	Kozai form of the Mean Motion
μ	Earth's gravitational constant
J_2	Zonal harmonic coefficient in geopotential
$R_\oplus$	Nominal radius of the Earth
t	Time
ψ	ηt
U	Geopotential
θ	Angle between XY inertial plane and satellite 1's radius vector
$\hat{X}$, $\hat{Y}$, $\hat{Z}$	Inertial coordinates
$\hat{P}$, $\hat{Q}$, $\hat{W}$	Intermediate inertial coordinates
$\hat{r}$, $\hat{i}$, $\hat{n}$	Local rotating coordinates
$[T]$	Transformation matrix from rotating frame to inertial frame
$\bar{R}$	Inertial radius vector to host satellite

$\bar{V}$	Inertial velocity vector of host satellite
$\bar{r}$	Local radius vector to 2nd satellite from host
$\bar{v}$	Local velocity vector of 2nd satellite
n	Vector of random numbers between -0.5 to 0.5
u	Zero-mean, white Gaussian noise
$\mathbf{P}$	Covariance matrix
$\mathbf{Q}_d$	Covariance of the dynamics noise
$\hat{x}(t_i^-)$	Estimated state after time propagation
$\hat{x}(t_i^+)$	Estimated state after the measurement update
$\mathbf{G}_d$	Identity matrix for this equivalent-discrete-time representation of a continuous-time system
Φ	State transition matrix
$\hat{x}$	Filter state
z	Range data
$\mathbf{h}$	Observation relation expectation of range data
$\mathbf{H}$	Linearized observation relation, $\mathbf{h}$
$\mathbf{K}$	Kalman filter gain
$\mathbf{R}$	Covariance of range noise
y	Elements of state to be compared, extracted by $\mathbf{C}$

C	3-by-6 matrix with 3-by-3 identity partition corresponding to the elements of the state to be compared, and a 3-by-3 zero matrix partition

Subscripts:

$\hat{X}$, $\hat{Y}$, $\hat{Z}$	Vectors expressed in inertial frame
$\hat{r}$, $\hat{i}$, $\hat{n}$	Vectors expressed in rotating frame
1, 2	Specify satellite
E	Estimator reference
T	Truth model reference
REL	Relative radius and velocity ($v - \omega X r$)
n	Sample time index in truth model
i, i-1	Current sample time and previous sample time in filter
d	Dynamics reference
k	Local iteration count
N	Final local iteration
rms	Root mean square

Superscripts:

-	Current sample time prior to data update
+	Current sample time after data update

Abstract

Previous work in the area of estimation of relative positions within a satellite cluster showed favorable results. However, the work was done using point mass orbits in the truth model. This thesis investigates the estimation of relative satellite positions operating in near circular orbit including the J_2 term in Earth's geopotential. The iterated, extended Kalman filter is used as the on-board estimator in order to gain better performance in the face of the non-linearities. The dynamics in the estimator are based on the Clohessy-Wiltshire equations for relative orbital motion. Inputs to the host estimator are range measurements from each satellite in the cluster. The relative position to the host satellite is investigated. A comparison of the true error and the rms covariance was performed.

NAVIGATION OF A SATELLITE CLUSTER WITH REALISTIC DYNAMICS

I. Introduction

Past studies have shown the feasibility of using a recursive filter for on-board estimators to determine the relative positions of satellites for use as a space based radar system [5,7,10]. Good results were obtained using two-body point mass astrodynamics and an on-board estimation model with the dynamics based on the Clohessy-Wiltshire equations.

The initial work at AFIT was done by Captain Michael Ward using the U-D covariance factorization Kalman filter with the Clohessy-Wiltshire equations. However, he encountered observability problems in the down range state component [10:2-17]. Further investigation into the observability problem was conducted by Captain Sherrie Norton Filer [5] and Captain Stephen Johnston [7]. Captain Filer obtained mixed results from her investigation into unobservable states. Captain Johnston furthered the effort and realized the Clohessy-Wiltshire equations could not determine the position and velocity of each satellite from the

origin on the reference orbit based on range measurements between the satellites. Only relative position and velocity could be determined from the host satellite to each other satellite [7:29]. The host satellite considers itself the center of the coordinate frame. After this was identified and analysis done, the results were favorable. He obtained 3 cm accuracy, well beyond the 25 m requirement.

However, the *truth* dynamics were based on a homogeneous, spherical Earth; effectively treating the Earth as having point mass gravity. This ignores one of the most dominant perturbative influences of a satellite's orbit. The Earth's rotation produces a bulge at the equator and large structures such as mountain ranges produce variations in the local mass. The effect of this oblateness and non-homogeneity is a non-uniform gravitational field. Although other effects are present as well, such as air drag and solar pressure, this thesis employs a *truth* model which accounts for the non-uniform gravity field only.

This thesis investigates the estimation of relative satellite motion in the presence of these *real* dynamics. The *truth* model computer program was developed to include the J2 term of Earth's geopotential. Since there are significant non-linearities between the *truth* dynamics and the estimator dynamics, the estimator developed was the iterated, extended Kalman filter [9:58].

The nominal orbital altitude (1000 km), cluster radius (500 meters), and accuracy requirements (25 meters) remain the same as the previous investigations [10:1-1,App A]. The accuracy is based on the requirement of the radar to form a

cohesive image using the combined data from each satellite. In order to achieve this, the relative position of each satellite must be known to at least one quarter of the radar wavelength [10:1-1].

The initial concept employed a cluster of up to 10 satellites orbiting in near circular, low Earth orbit. Capt Johnston realized each satellite's relative state was independent of the other [7:29]. Therefore, only a two satellite cluster will be investigated. The procedure can be generalized to include more satellites in the cluster.

In this work, the origin of the rotating reference frame is centered on satellite # 1 which will contain the on-board estimator being investigated. The truth model is the ruler against which the estimator is placed. A comparison of true error and rms covariance will be made [8:337].

II. Background

The fundamental purpose of this investigation is to compare the estimation with *real* dynamics. This is done by generating a truth model based on *real* dynamics and comparing with the results achieved from the filter's estimation of the state. In this way, the same mission can be run over and over with different random noise in the range to analyze the filter's performance.

The truth model computer program was written to include the J_2 term of Earth's geopotential. The J_2 term is the most dominant term in the geopotential, beyond the Newtonian point mass orbit potential. It accounts for both periodic and secular variations in an orbit. The J_2 effects cause the secular variations to be the dominant perturbation source in the Mean Anomaly, M, Argument of Perigee, ω, and the Right Ascension of the Ascending Node, Ω, near 1000 km. Figure 1 and Figure 2 show the Newtonian (constant) value, the theoretically predicted secular variation and the actual secular variation in ω and Ω respectively.

The predicted secular variations are given by [4:369]:

$$\omega = \omega_0 + \dot{\omega} t = \omega_0 + \frac{3\eta J_2 R_\oplus^2 t}{2a^2(1 - e^2)^2}\left(2 - \tfrac{5}{2}\sin^2 i\right)$$
$$\Omega = \Omega_0 + \dot{\Omega} t = \Omega_0 - \frac{3\eta J_2 R_\oplus^2 t}{2a^2(1 - e^2)^2}\cos i \qquad (1)$$

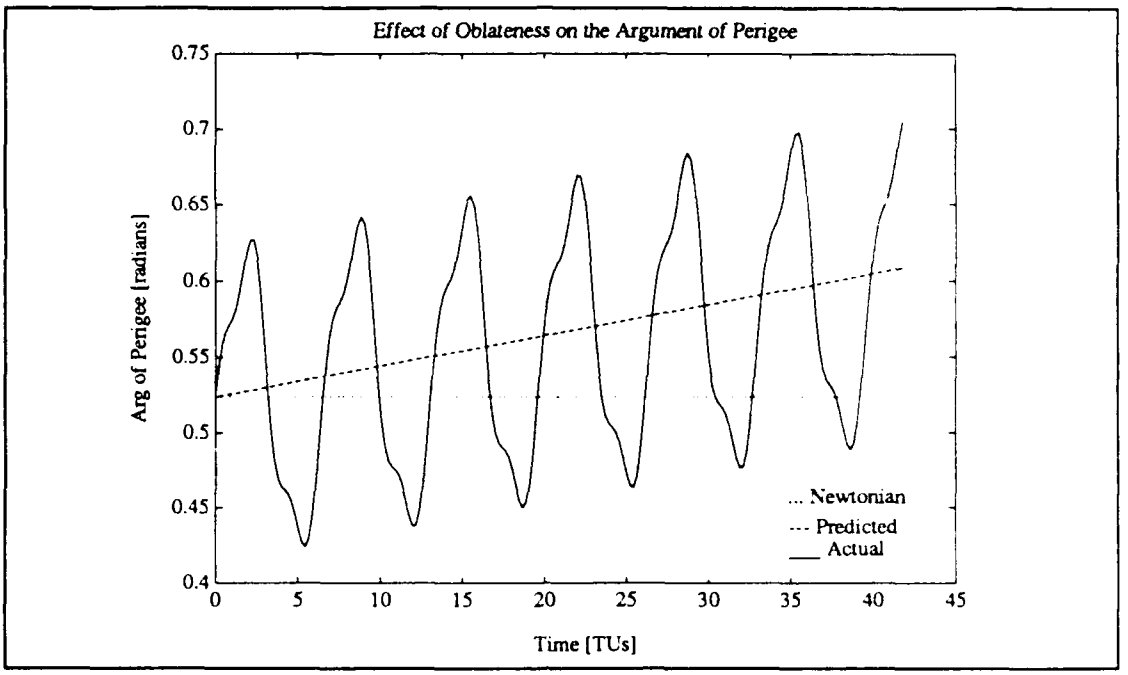

Figure 1. Comparison of the Newtonian, predicted and actual secular variation in the Argument of Perigee, ω, due to J_2.

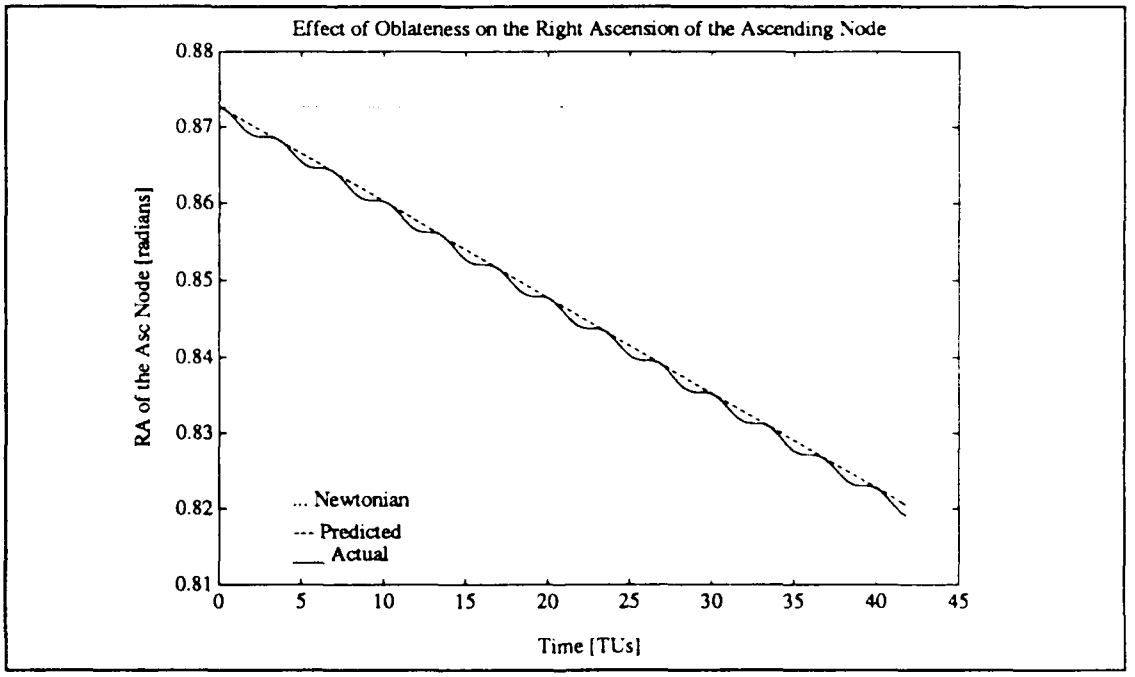

Figure 2. Comparison of Newtonian, predicted, and actual secular variation in the Right Ascension of the Ascending Node, Ω, due to J_2.

where:

η = Mean Motion

J_2 = Zonal harmonic coefficient of the geopotential

a = Semi-major axis

e = Eccentricity

i = Inclination of the orbit

The actual secular variation shows oscillations periodic with the orbit. This is due to the periodic variations in a, e and i of the orbit due to J_2. These plots verify the proper functioning of the orbit determination part of the truth model. The actual variations with the periodicity in the orbit follow the predicted variations as expected.

The estimator computer program was written as an iterated, extended Kalman filter employing the Clohessy-Wiltshire equations for the dynamics to predict the state. It uses range measurements from the truth model to update the predicted state. The truth model generates the relative position and velocity of the cluster and provides the estimator with inputs of range corrupted with white Gaussian noise. The estimator uses these inputs to generate its correction to the relative position elements of the state. It also generates an estimate of its error, the covariance. This covariance is compared to the true error to allow tuning the filter.

2.1 Truth Model

2.1.1 Coordinate Frame Definition

The problem is presented using three coordinate frames. Two of these frames will be employed through out the thesis and one serves only to ease the set-up of the initial conditions of the second satellite. The frames are; the inertial frame centered on the Earth, the rotating frame centered on the host satellite, and the third is the inertial frame aligned with the rotating frame.

The first frame is referenced in the truth model. The equations of motion in the truth model for each satellite are defined in the inertial frame with components ($\hat{X}$, $\hat{Y}$, $\hat{Z}$). $\hat{X}$ is aligned with the First Point of Aries (Υ), $\hat{Z}$ the rotation axis of the Earth, and $\hat{Y}$ completes the right hand orthogonal set.

The second frame, the rotating frame, is fixed to satellite 1. It has components, ($\hat{r}$, $\hat{i}$, $\hat{n}$) where, $\hat{r}$ is along the radius vector from the center of the Earth to satellite 1, $\hat{n}$ is perpendicular to the orbital plane and $\hat{i}$ completes the right hand orthogonal set. This frame is the frame referenced in the estimator. Once satellite 2's position is found inertially, the relative position from satellite 1 is found and transformed into the rotating frame.

The third frame is only used to define the initial inertial conditions of satellite 2 using the Clohessy-Wiltshire equations to provide appropriate initial velocities.

This frame is simply the inertial frame ($\hat{X}$, $\hat{Y}$, $\hat{Z}$) rotated to align with the rotating frame and has components ($\hat{P}$, $\hat{Q}$, $\hat{W}$). After the initial conditions are specified only the inertial ($\hat{X}$, $\hat{Y}$, $\hat{Z}$) and the rotating ($\hat{r}$, $\hat{i}$, $\hat{n}$) frames will be used. Figure 3 illustrates these frames.

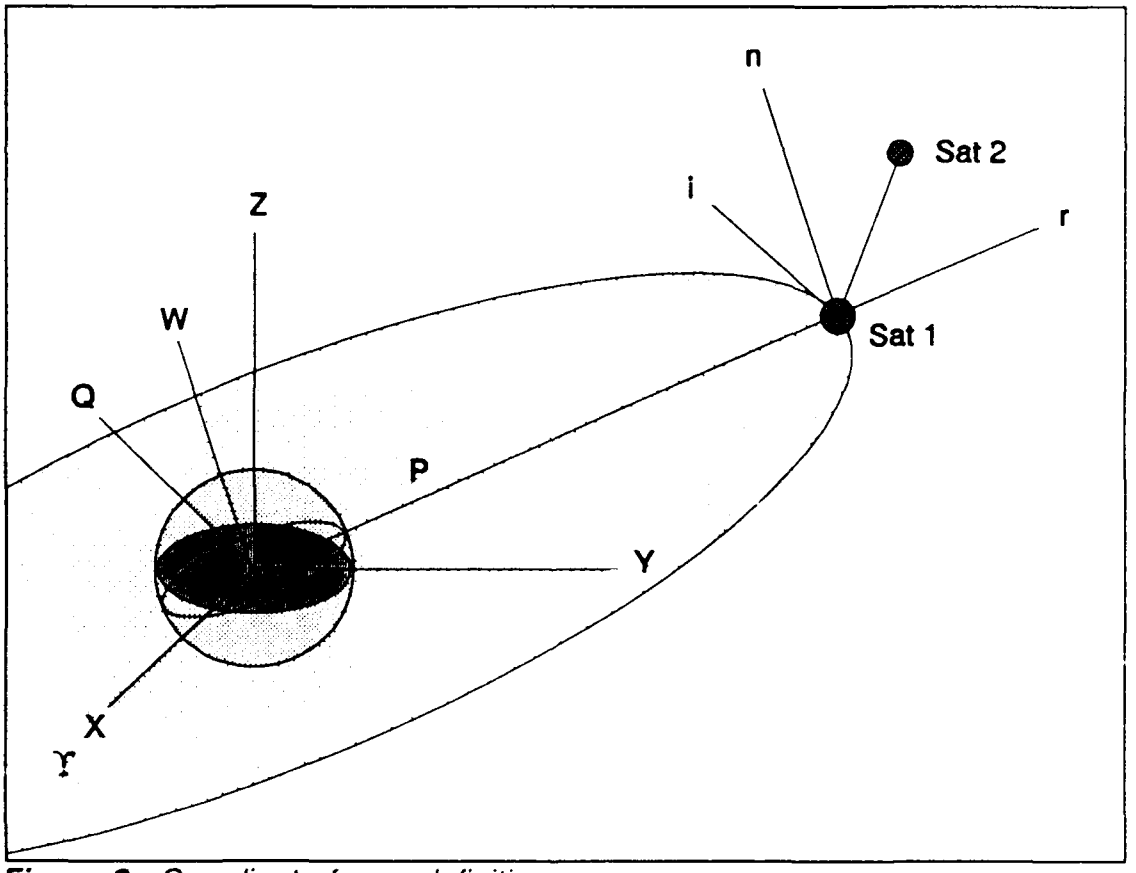

Figure 3. Coordinate frame definition.

2.1.2 Initial Conditions

Initial conditions are specified by a reference orbit for the host satellite and specifying the relative state of satellite 2. Once a reference orbit is specified for satellite 1, the host, satellite 2's initial relative state is defined in the rotating frame. Satellite 1's initial state is defined in the inertial frame and expressed in the rotating frame. This initializes satellite 1's state in the truth model and the filter. Satellite 2's initial state is defined in the rotating frame about satellite 1. Its state is also expressed in the inertial frame. This initializes both the truth and filter models for satellite 2.

The initial position and velocity of satellite 1, and therefore the rotating reference frame, are arbitrarily chosen to have the following classical elements, a=1.156784906 (1000 km altitude), e=0.00011, i=28.5°, ω=30°, Ω=50° and ν=0°. The initial location of this rotating frame in the inertial frame ($\hat{X}$, $\hat{Y}$, $\hat{Z}$) is easily obtained from the classical elements [1:71,82] via the ($\hat{P}$, $\hat{Q}$, $\hat{W}$) frame.

The position and velocity in the $\hat{P}$, $\hat{Q}$, $\hat{W}$ frame are expressed as:

$$\mathbf{r} = r\cos\nu\,\hat{P} + r\sin\nu\,\hat{Q} \tag{2}$$

$$\mathbf{v} = \left(\frac{\mu}{a(1-e^2)}\right)^{1/2}[-\sin\nu\,\hat{P} + (e+\cos\nu)\,\hat{Q}] \tag{3}$$

These are rotated into the inertial frame ($\hat{X}$, $\hat{Y}$, $\hat{Z}$) by:

$$\begin{bmatrix} r_X \\ r_Y \\ r_Z \end{bmatrix} = \mathbf{R} \begin{bmatrix} r_P \\ r_Q \\ r_W \end{bmatrix} \quad \text{and} \quad \begin{bmatrix} v_X \\ v_Y \\ v_Z \end{bmatrix} = \mathbf{R} \begin{bmatrix} v_P \\ v_Q \\ v_W \end{bmatrix} \tag{4}$$

where,

$$\mathbf{R} = \begin{bmatrix} \cos\Omega\cos\omega - \sin\Omega\sin\omega\cos i & -\cos\Omega\sin\omega - \sin\Omega\cos\omega\cos i & \sin\Omega\sin i \\ \sin\Omega\cos\omega + \cos\Omega\sin\omega\cos i & -\sin\Omega\sin\omega + \cos\Omega\cos\omega\cos i & -\cos\Omega\sin i \\ \sin\omega\sin i & \cos\omega\sin i & \cos i \end{bmatrix} \tag{5}$$

With the classical elements given above, the initial position and velocity of the rotating frame expressed in the inertial frame in canonical units are:

$$\bar{R}_1 = \begin{Bmatrix} 0.25453861 \\ 1.09403658 \\ 0.27595466 \end{Bmatrix} \text{ DU} \tag{6}$$

$$\bar{V}_1 = \begin{Bmatrix} -0.84098533 \\ 0.09874202 \\ 0.38425099 \end{Bmatrix} \frac{\text{DU}}{\text{TU}} \tag{7}$$

where, 1 DU = 6378.145 km and 1 TU = 806.8118744 secs. These are found by defining Earth's gravitational constant, $\mu_\oplus = 1\ DU^3/TU^2 = 3.986012 \times 10^5$ km^3/sec^2.

Since the rotating frame is in a near-circular orbit (e=.00011), the transformation, $[T]$, from the inertial frame ($\hat{X}$, $\hat{Y}$, $\hat{Z}$) to the rotating frame ($\hat{r}$, $\hat{i}$, $\hat{n}$) is determined from the host satellite's position and velocity:

$$\begin{Bmatrix} \hat{r} \\ \hat{i} \\ \hat{n} \end{Bmatrix} = [\,T\,] \begin{Bmatrix} \hat{X} \\ \hat{Y} \\ \hat{Z} \end{Bmatrix} = \begin{bmatrix} T_r \\ T_i \\ T_n \end{bmatrix} \begin{Bmatrix} \hat{X} \\ \hat{Y} \\ \hat{Z} \end{Bmatrix} \tag{8}$$

where,

$$\begin{aligned} [T_r] &= \left[\frac{\bar{R}}{|\bar{R}|} \right]_{[\hat{X},\hat{Y},\hat{Z}]} \\ [T_i] &= [T_n] \times [T_r] \\ [T_n] &= \left[\frac{\bar{R} \times \bar{V}}{|\bar{R} \times \bar{V}|} \right]_{[\hat{X},\hat{Y},\hat{Z}]} \end{aligned} \tag{9}$$

and $\bar{R}$ and $\bar{V}$ are the radius and velocity of satellite 1 in the inertial coordinates.

The position elements of satellite 2's state are randomly placed about the rotating origin:

$$\bar{r}_2 = \{n_2\} * (500\,\text{meters}) \tag{10}$$

where n_2 is a vector of random numbers between -0.5 and 0.5.

It is rotated into the inertial frame ($\hat{X}$, $\hat{Y}$, $\hat{Z}$) to be used by the truth model. The position of satellite 2 in the inertial frame is found by:

$$\bar{R}_{2[\hat{X},\hat{Y},\hat{Z}]} = [T]^T \bar{r}_{2[\hat{r},\hat{i},\hat{n}]} \tag{11}$$

With the position of satellite 2 specified in both frames, the velocity is defined using the Clohessy-Wiltshire equations. The Clohessy-Wiltshire equations (see Section 2.2.1) allow appropriate values for radial and out-of-plane velocity components in the ($\hat{P}$, $\hat{Q}$, $\hat{W}$) frame. Both the radial and out-of-plane velocity components are found by multiplying the relative distance expression by the mean motion of the reference orbit and then equating to the relative velocity expression. Since this frame is initially aligned with the rotating reference frame,

$$V_2 \hat{P} = \eta r_2 \hat{P} \tag{12}$$

$$V_2 \hat{W} = \eta r_2 \hat{W} \tag{13}$$

where η = the mean motion of the reference trajectory.

In order to maintain cluster integrity by reducing drift, the orbital periods of each satellite must be the same. The orbital period in the two-body Newtonian point mass orbit is a function of the semi-major axis only and completely removes

drift. Letting this be the starting point for the perturbed orbit, the two-body energy equation is used to determine the third component of the velocity. Utilizing this equation and assuming the semi-major axis is constant and the geopotential is based on a point mass yields:

$$V_2\,\hat{Q} = \left\{2\mu\left(\frac{1}{R_2} - \frac{1}{2a}\right) - (V_2 \cdot V_2)\hat{P} - (V_2 \cdot V_2)\hat{W}\right\}^{1/2} \hat{Q} \qquad (14)$$

These velocity components are expressed in the rotating frame to be used by the estimator as follows:

$$\bar{V}_{2rel[\hat{r},\hat{i},\hat{n}]} = \bar{V}_{2[\hat{r},\hat{i},\hat{n}]} - (\bar{\omega} \times \bar{r}_2)_{[\hat{r},\hat{i},\hat{n}]} \qquad (15)$$

where, initially, $\bar{V}_{2[\hat{r},\hat{i},\hat{n}]} = (\bar{V}_2 - \bar{V}_1)_{[\hat{P},\hat{Q},\hat{W}]}$.

The velocity components are expressed in the inertial frame to initialize the truth model by

$$\bar{V}_{2[\hat{X},\hat{Y},\hat{Z}]} = [T]^T \bar{V}_{2[\hat{P},\hat{Q},\hat{W}]} \qquad (16)$$

Therefore, the initial state to the estimator is

$$\bar{x}_E(0) = \left\{ \begin{matrix} \bar{r}_2 \\ \bar{v}_2 \end{matrix} \right\}_{[r,i,n]} \tag{17}$$

and the initial state to the truth model is

$$\bar{X}_T(0) = \left\{ \begin{matrix} \bar{R}_1 \\ \bar{V}_1 \\ \bar{R}_2 \\ \bar{V}_2 \end{matrix} \right\}_{[X,Y,Z]} \tag{18}$$

2.1.3 Dynamics

Having defined the initial conditions, the truth model state must be found at subsequent times. Previous studies used Newtonian point mass dynamics for the truth model. As addressed above, this maintained the cluster's integrity well. However, the Earth *is* non-spnerical and non-homogeneous, which causes drift to appear in the *real* dynamics. Orbits based on the point mass relative dynamics and the Clohessy-Wiltshire dynamics retrace themselves since there is no perturbations present. Figure 4 is a plot of 10 orbits of both the point mass relative dynamics and the Clohessy-Wiltshire dynamics. There is no perceptible difference after 10 orbits. Figure 5 shows the distinct difference in the relative

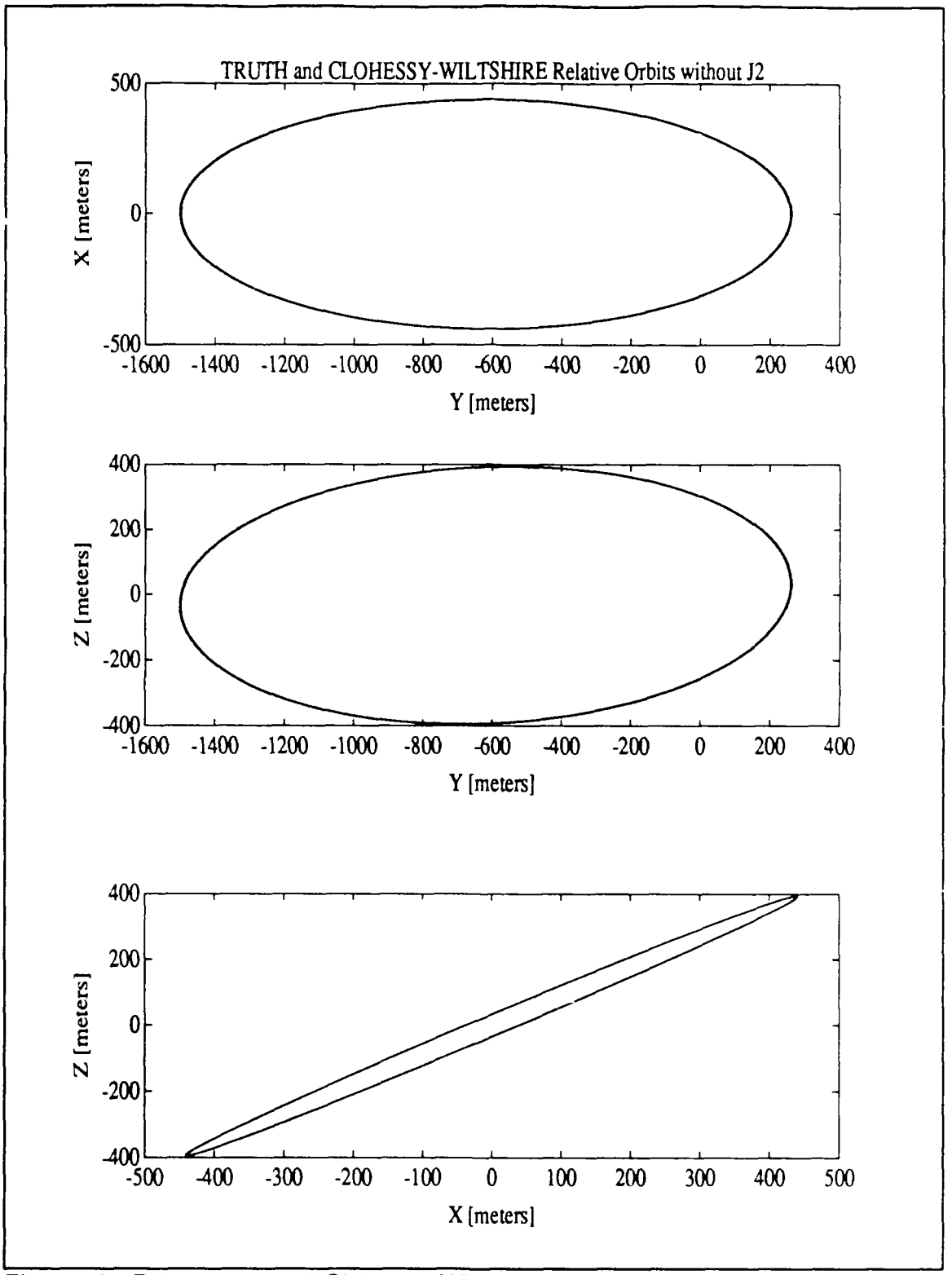

Figure 4. Point mass and Clohessy-Wiltshire orbits (10 orbits).

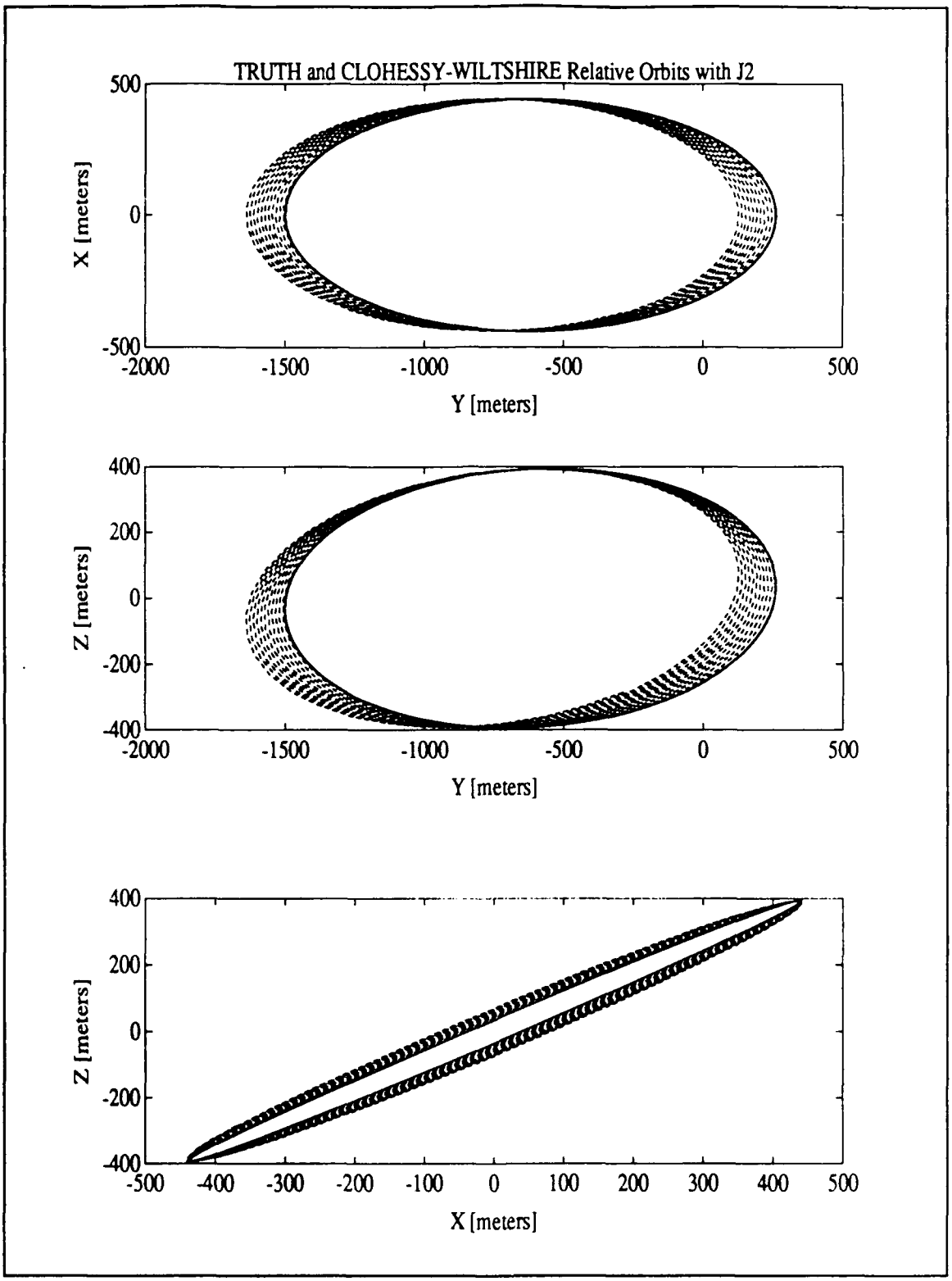

Figure 5. *Real* dynamics and Clohessy-Wiltshire orbits (10 orbits).

orbits of the *real* dynamics and the Clohessy-Wiltshire dynamics. Later this will play an important factor in the performance analysis.

This difference is due to the oblateness of the Earth and the gravitational potential. The Earth's geopotential including the J_2 zonal harmonic term and neglecting the other non-vanishing higher order terms is [12:84]:

$$U = \frac{\mu}{R} - \frac{\mu}{R}\left(\frac{R_\oplus}{R}\right)^2 \frac{1}{2}(3\cos^2\theta - 1)J_2 \tag{19}$$

where:

$$\begin{aligned} R &= (X^2+Y^2+Z^2)^{1/2} \\ \cos\theta &= \frac{Z}{R} \\ R_\oplus &= \text{radius of the Earth} \\ \mu &= \text{Earth's gravitational constant} \end{aligned} \tag{20}$$

The truth model uses the potential of Eq (19) expressed in the inertial frame as

$$U = \frac{\mu}{(X^2+Y^2+Z^2)^{1/2}} - \frac{J_2 \mu R_\oplus^2}{2(X^2+Y^2+Z^2)^{3/2}}\left(\frac{3Z^2}{X^2+Y^2+Z^2} - 1\right) \tag{21}$$

With J_2 set to 0, the geopotential is simply the Newtonian point mass potential.

The future position and velocity of satellites 1 and 2 are determined inertially by numerically integrating the equations of motion. Integration is done using a predictor-corrector routine called HAMING [12:110] (see Appendix A). HAMING requires a subroutine called RHS (Right Hand Side). This subroutine contains the right hand side of the state-differential equations of motion:

$$
\begin{aligned}
\dot{X} &= V_x \\
\dot{Y} &= V_y \\
\dot{Z} &= V_z \\
\ddot{X} = \dot{V}_x &= \frac{\partial U}{\partial X} = -\frac{\mu X}{R^3}\left[1 - \frac{3}{2}\frac{J_2 R_\oplus^2}{R^2}\left(\frac{5Z^2}{R^2} - 1\right)\right] \\
\ddot{Y} = \dot{V}_y &= \frac{\partial U}{\partial Y} = -\frac{\mu Y}{R^3}\left[1 - \frac{3}{2}\frac{J_2 R_\oplus^2}{R^2}\left(\frac{5Z^2}{R^2} - 1\right)\right] \\
\ddot{Z} = \dot{V}_z &= \frac{\partial U}{\partial Z} = -\frac{\mu Z}{R^3}\left[1 + \frac{3}{2}\frac{J_2 R_\oplus^2}{R^2}\left(3 - \frac{5Z^2}{R^2}\right)\right]
\end{aligned}
\tag{22}
$$

A sample rate for the estimator is preselected in order to generate range data for the estimator. The sample rate determines how frequently the states of satellites 1 and 2 will be used to calculate the range provided to the estimator. At each of these sample times the relative state for satellite 2 is determined by:

$$
\begin{aligned}
\bar{R}_{rel[\hat{X},\hat{Y},\hat{Z}]} &= \left\{\bar{R}_2(t) - \bar{R}_1(t)\right\} \\
\bar{V}_{rel[\hat{X},\hat{Y},\hat{Z}]} &= \left\{\bar{V}_2(t) - \bar{V}_1(t)\right\}
\end{aligned}
\tag{23}
$$

The coordinate transformation matrix, $[T]$, is re-evaluated by Eq (9). The relative position and velocity are rotated into the rotating frame as follows:

$$\left\{ \begin{matrix} \bar{r} \\ \bar{v} \end{matrix} \right\}_{rel[\hat{r},\hat{i},\hat{n}]} = \left\{ \begin{matrix} \bar{r} \\ \bar{v} - (\bar{\omega} \times \bar{r}) \end{matrix} \right\}_{[\hat{r},\hat{i},\hat{n}]} \tag{24}$$

where,

$$\left\{ \begin{matrix} \bar{r} \\ \bar{v} \end{matrix} \right\}_{[\hat{r},\hat{i},\hat{n}]} = [\,T\,]^T \left\{ \begin{matrix} \bar{R} \\ \bar{V} \end{matrix} \right\}_{rel[\hat{X},\hat{Y},\hat{Z}]} \tag{25}$$

Finally, the *truth* model generates the range measurement for the estimator by

$$z_n = |\bar{r}_{2rel[\hat{r},\hat{i},\hat{n}]}| + u_n \tag{26}$$

where u_n is a zero-mean, white Gaussian noise with its associated covariance of R_n [8:330]. The noise is the representation of measurement inaccuracies as well as other error sources [10:2-6].

2.2 Filter Model

The choice of the iterated, extended Kalman filter was made in light of the significance of the non-linearities of the system, both in the observation relationship and the dynamics [9:58]. The iteration occurs at each data sample in order to

modify the reference trajectory with a better estimate of the state. After convergence, which was chosen to be a difference of 0.0001 in each iterated position element, or a specified number of iterations, chosen to be 8, the final reference state is deemed the new estimate with its associated covariance.

One potential problem with the Kalman filter is "starting" the filter, since the first time propagation occurs before any data is sampled. Therefore, the initial state is considered known from the truth model as described in Section 2.1.2. The initial covariance, P_0, must also be specified. P_0 will be considered diagonal with initial position and velocity covariance of 25 m^2 and 1 $(m/s)^2$, respectively. These result from an assumption of an initial position accuracy of 5 *m* and velocity accuracy of 1 *m/s*. These will be replaced with more appropriate values as the filter is tuned.

2.2.1 Dynamics (Clohessy-Wiltshire Equations)

The state is propagated forward to the time of next data acquisition. Since the dynamics, governed by the Clohessy-Wiltshire equations, are linear (see below), the state and covariance propagation are defined by [8:220]:

$$\hat{x}(t_i^-) = \Phi(t_i, t_{i-1})\ \hat{x}(t_{i-1}^+) \tag{27}$$

$$\mathbf{P}(t_i^-) = \Phi(t_i, t_{i-1})\mathbf{P}(t_{i-1}^+)\Phi^T(t_i, t_{i-1}) + \mathbf{G}_d(t_{i-1})\mathbf{Q}_d(t_{i-1})\mathbf{G}_d^T(t_{i-1}) \quad (28)$$

where,

$\mathbf{Q}_d$ is the covariance of the dynamics noise.

$\hat{x}(t_i^-)$ is the estimated state after time propagation.

$\hat{x}(t_i^+)$ is the estimated state after the measurement update.

$\mathbf{G}_d$ is the identity matrix for this equivalent-discrete-time representation of a continuous-time system [8:377].

Φ is the state transition matrix.

The state is propagated to time (t_i^-) by means of Φ:

$$\Phi \equiv \frac{\partial \hat{x}(t_i)}{\partial \hat{x}(t_0)} \quad (29)$$

Figure 6 illustrates the state propagation and data acquisition [8:207].

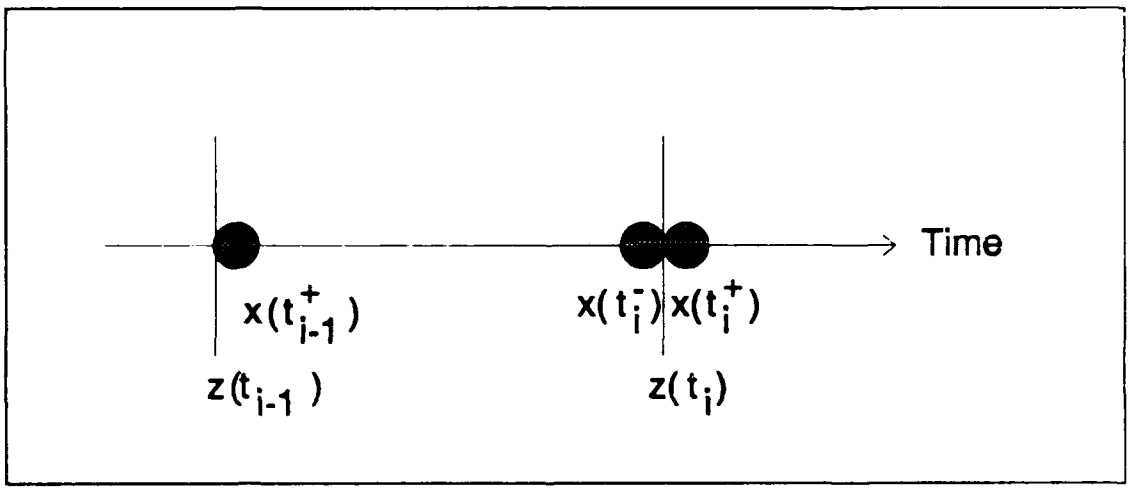

Figure 6. State propagation and update.

The equations of relative motion used to develop the Clohessy-Wiltshire equations are defined as follows [13:80]:

$$\delta\ddot{r} - 2\eta r_0 \delta\dot{\theta} - 3\eta^2 \delta r = 0 \tag{30}$$

$$r_0 \delta\ddot{\theta} + 2\eta \delta\dot{r} = 0 \tag{31}$$

$$\delta\ddot{z} + \eta^2 \delta z = 0 \tag{32}$$

where, δr, $r_0\delta\theta$, and δz are the $\hat{r}$, $\hat{i}$, $\hat{n}$ coordinates respectively.

These coordinates will be defined as x, y, and z for the remainder of the thesis. It should be noted, these are a first order form of the Newtonian point mass relative equations of motion.

Eqs (30), (31), and (32) are readily integrated since they are a set of linear, constant-coefficient differential equations. Applying the initial conditions,

$$\mathbf{x}(0) = \begin{Bmatrix} x_0 \\ y_0 \\ z_0 \end{Bmatrix}, \quad \dot{\mathbf{x}}(0) = \begin{Bmatrix} \dot{x}_0 \\ \dot{y}_0 \\ \dot{z}_0 \end{Bmatrix}$$

the solutions are [13:80-81]:

$$x(t) = -\left(\frac{2}{\eta}\dot{y}_0 + 3x_0\right)\cos \eta t + \frac{\dot{x}_0}{\eta}\sin \eta t + 4x_0 + \frac{2}{\eta}\dot{y}_0 \tag{33}$$

$$y(t) = y_0 - (3\dot{y}_0 + 6\eta x_0)t + \left(\frac{4\dot{y}_0}{\eta} + 6x_0\right)\sin \eta t + \frac{2\dot{x}_0}{\eta}\cos \eta t - \frac{2\dot{x}_0}{\eta} \tag{34}$$

$$z(t) = z_0 \cos \eta t + \frac{\dot{z}_0}{\eta}\sin \eta t \tag{35}$$

$$\dot{x}(t) = (2\dot{y}_0 + 3\eta x_0)\sin \eta t + \dot{x}_0 \cos \eta t \tag{36}$$

$$\dot{y}(t) = (-3\dot{y}_0 - 6\eta x_0) + (6\eta x_0 + 4\dot{y}_0)\cos \eta t - 2\dot{x}_0 \sin \eta t \tag{37}$$

$$\dot{z}(t) = -z_0 \eta \sin \eta t + \dot{z}_0 \cos \eta t \tag{38}$$

Now the state transition matrix is determined by Eq (29):

$$\Phi = \begin{bmatrix} 4-3\cos\psi & 0 & 0 & \frac{1}{\eta}\sin\psi & \frac{2}{\eta}(1-\cos\psi) & 0 \\ 6(\sin\psi-\psi) & 1 & 0 & \frac{2}{\eta}(\cos\psi-1) & \frac{4}{\eta}\sin\psi-\frac{3}{\eta}\psi & 0 \\ 0 & 0 & \cos\psi & 0 & 0 & \frac{1}{\eta}\sin\psi \\ 3\eta\sin\psi & 0 & 0 & \cos\psi & 2\sin\psi & 0 \\ 6\eta(\cos\psi-1) & 0 & 0 & -2\sin\psi & -3+4\cos\psi & 0 \\ 0 & 0 & -\eta\sin\psi & 0 & 0 & \cos\psi \end{bmatrix} \quad \textbf{(39)}$$

where, $\psi = \eta t$ and t is the sample time.

The state is propagated to the new data acquisition time by Eq (27), and in general, Eq (27) becomes:

$$\hat{x}(t_i^-) = \begin{bmatrix} \Phi_2 & 0 & \cdots & 0 \\ 0 & \Phi_3 & \cdots & 0 \\ \vdots & \vdots & \ddots & \vdots \\ 0 & 0 & \cdots & \Phi_{s-1} \end{bmatrix} \begin{Bmatrix} \hat{x}_2(t_{i-1}^+) \\ \hat{x}_3(t_{i-1}^+) \\ \vdots \\ \hat{x}_{s-1}(t_{i-1}^+) \end{Bmatrix} \quad \textbf{(40)}$$

where the subscripts reference each satellite in the cluster.

Φ need only be evaluated once given the sample interval, (t_{i-1}) to (t_i) . This is one of the major benefits of linear dynamics.

2.2.2 Iterated, Extended Kalman Filter

With the initial state and covariance propagated to time (t_i), the measurement update, $\mathbf{z}_i$, is incorporated by means of the state and covariance update equations. Data is typically not a scalar, and therefore the expectation of the data is typically a vector and is denoted by **h**. The bold notation is retained for both the data and its expectation for the remainder of the thesis. Since $\mathbf{z}_i$ is the range, it is expected to be of the form of **h**, which is defined as

$$\mathbf{h} = \{x_2^2 + y_2^2 + z_2^2\}^{1/2} \tag{41}$$

In general, **h** becomes

$$\mathbf{h} = \begin{Bmatrix} \{x_2^2 + y_2^2 + z_2^2\}^{1/2} \\ \vdots \\ \{x_s^2 + y_s^2 + z_s^2\}^{1/2} \end{Bmatrix} = \begin{Bmatrix} \mathbf{h}_1 \\ \vdots \\ \mathbf{h}_{s-1} \end{Bmatrix} \tag{42}$$

where, x, y, and z are the components in the ($\hat{r}$, $\hat{i}$, $\hat{n}$) frame.

The expectation, **h**, is linearized and evaluated at $\hat{x}(t_i^-)$ by

$$\mathbf{H} \equiv \left.\frac{\partial \mathbf{h}}{\partial \mathbf{x}}\right|_{\mathbf{x}=\hat{\mathbf{x}}(t_i^-)} \tag{43}$$

which becomes

$$\mathbf{H} = \begin{bmatrix} \frac{x}{h} & \frac{y}{h} & \frac{z}{h} & 0 & 0 & 0 \end{bmatrix} \tag{44}$$

In general, **H** has the form

$$\mathbf{H} = \begin{bmatrix} \mathbf{H}_2 & 0 & 0 & \cdots & 0 \\ 0 & \mathbf{H}_3 & 0 & \cdots & 0 \\ \vdots & \vdots & \vdots & \ddots & 0 \\ 0 & 0 & 0 & \cdots & \mathbf{H}_{s-1} \end{bmatrix} \tag{45}$$

where,

$$\mathbf{H}_{s-1} = \begin{bmatrix} \frac{x_{s-1}}{h_{s-1}} & \frac{y_{s-1}}{h_{s-1}} & \frac{z_{s-1}}{h_{s-1}} & 0 & 0 & 0 \end{bmatrix} \tag{46}$$

The state update is given by [9:59]:

$$\hat{\mathbf{x}}_{k+1} = \hat{\mathbf{x}}(t_i^-) + \mathbf{K}(t_i)\left\{\mathbf{z}_i - \mathbf{h}(\hat{\mathbf{x}}_k, t_i) - \mathbf{H}(\hat{\mathbf{x}}_k, t_i)\left[\hat{\mathbf{x}}(t_i^-) - \hat{\mathbf{x}}_k\right]\right\} \tag{47}$$

where,

$$\mathbf{K}(t_i) = \mathbf{P}(t_i^-)\mathbf{H}^T(\hat{\mathbf{x}}_k, t_i)\left[\mathbf{H}(\hat{\mathbf{x}}_k, t_i)\mathbf{P}(t_i^-)\mathbf{H}^T(\hat{\mathbf{x}}_k, t_i) + \mathbf{R}(t_i)\right]^{-1} \tag{48}$$

for k = 0, 1, 2, ..., N-1.

$\mathbf{R}(t_i)$ is the covariance of the noise in the data.

The iterated, extended Kalman filter update equations are a slightly modified form of the extended Kalman filter update equations [9:44,59]. The iterated method uses the updated state estimate $\hat{\mathbf{x}}(t_i^+)$, generated by the standard extended Kalman filter, "as a better state estimate than $\hat{\mathbf{x}}(t_i^-)$ for evaluating **h** and **H** in the measurement update relations" [9:58].

This is important since the **h** vector is the expectation of the data, $\mathbf{z}_i$, and is used to evaluate the residual,

$$\mathbf{r}_i = \mathbf{z}_i - \mathbf{h}(\hat{\mathbf{x}}(t)) \tag{49}$$

found in the state update equation, Eq (47).

It is seen that $\hat{x}_1$ is actually $\hat{x}(t_i^+)$ given by the standard Kalman filter [9:59]. When the specified number of iterations have been made or when $|\hat{x}_k - \hat{x}_{K+1}|$ is less than a predetermined amount, $\hat{x}_N$ is declared the new reference trajectory; that is,

$$\hat{x}(t_i^+) \equiv \hat{x}_N \tag{50}$$

The new reference trajectory is now permanently updated, with a covariance of

$$\mathbf{P}(t_i^+) = \mathbf{P}(t_i^-) - \mathbf{K}(t_i)\mathbf{H}\left[\hat{x}(t_i^-), t_i\right]\mathbf{P}(t_i^-) \tag{51}$$

This iterative method reevaluates the observation relations, **h** and **H**, with each $\hat{x}_k$ to achieve a better reference trajectory. This done to correct for the nonlinearities in the observation and the dynamics of the system.

III. Performance Analysis

3.1 Performance Evaluation

Assessment of the filter's performance is accomplished by comparing the true error and root mean square covariance [8:337]. By graphically comparing the true error and the root mean square covariance, the filter can be "tuned". This method of tuning will give a general assessment of the filter's capabilities of tracking the other satellites in the cluster.

In order to perform the comparison, the position elements of both models are extracted from the complete state by

$$\begin{aligned} \mathbf{y}_t &= \mathbf{C}_t \mathbf{x}_t \\ \hat{\mathbf{y}} &= \mathbf{C}\hat{\mathbf{x}} \end{aligned} \tag{52}$$

Since the states are the same for both models,

$$\mathbf{C} = \mathbf{C}_t = \begin{bmatrix} 1 & 0 & 0 & 0 & 0 & 0 \\ 0 & 1 & 0 & 0 & 0 & 0 \\ 0 & 0 & 1 & 0 & 0 & 0 \end{bmatrix} \tag{53}$$

The true error is depicted in Figure 7 and is defined as

$$\mathbf{e}_t = \hat{\mathbf{y}} - \mathbf{y}_t = \begin{bmatrix} x_f - x_t \\ y_f - y_t \\ z_f - z_t \end{bmatrix} \tag{54}$$

In order to effectively use the true error, its magnitude, $|\mathbf{e}_t|$, is compared with the rms of the trace of $\mathbf{P}_e$. $\mathbf{P}_e$ is given by

$$\mathbf{P}_e = \mathbf{C}\mathbf{P}\mathbf{C}^T \tag{55}$$

The root mean square of the trace of $\mathbf{P}_e$ is defined as

$$P_{rms} \equiv (\mathrm{tr}\mathbf{P}_e)^{1/2} = (\sigma_x^2 + \sigma_y^2 + \sigma_z^2)^{1/2} \tag{56}$$

where, σ^2 is the covariance for each diagonal position element. The true error and rms covariance will be utilized in Section 3.3 and following.

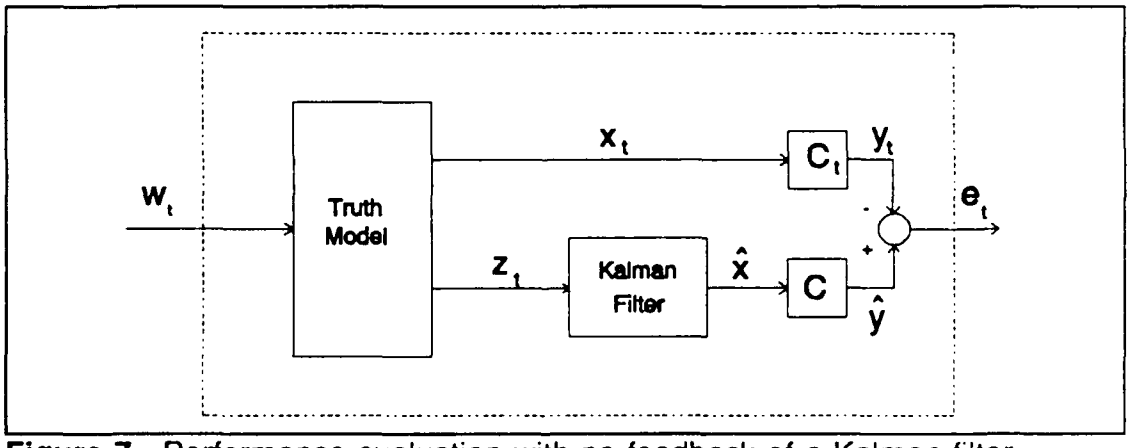

Figure 7. Performance evaluation with no feedback of a Kalman filter.

3.2 Truth Model Validation

The relative position part of the truth model was validated by running a launch trajectory from an orbiting vehicle as was done in [3:56]. The trajectory was a ΔV of 60 m/sec at a launch angle of 45° from a near circular orbit. The truth model orbit was given an eccentricity of 0.00011. Dunning compared the Clohessy-Wiltshire solution with the exact solution of the relative equations of motion. Figure 8 shows the same results as obtained in [3:56].

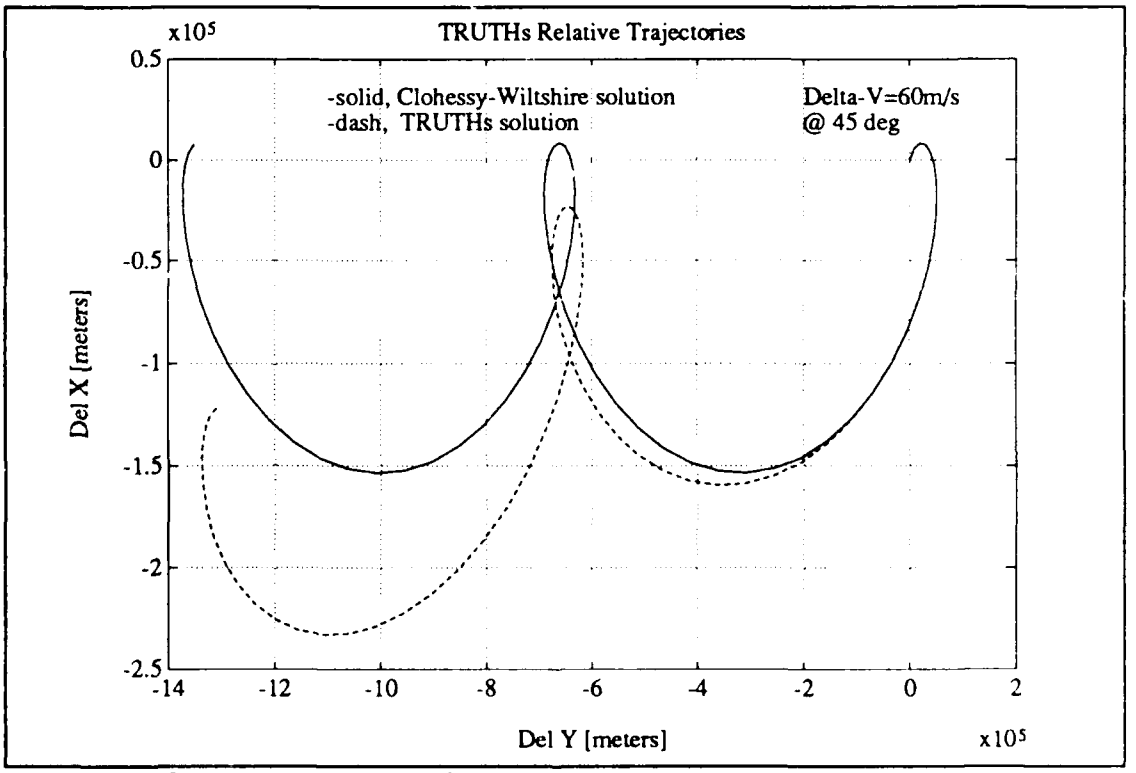

Figure 8. Comparison of the Clohessy-Wiltshire and truth model solutions.

3.3 Filter Model Validation

The filter's general behavior is determined by running it with no dynamics noise. This is accomplished by providing the filter with $\mathbf{Q}_d = 0$ and analyzing the behavior of the true error and the rms covariance. With $\mathbf{Q}_d = 0$, the true error, $|\mathbf{e}_t|$, and rms covariance, P_{rms}, were plotted and are shown in Figure 9.

As expected the true error diverges while the rms covariance converges toward zero since the filter has total confidence in its dynamics. This confidence will be tempered with dynamics noise in order to keep the filter's estimate from

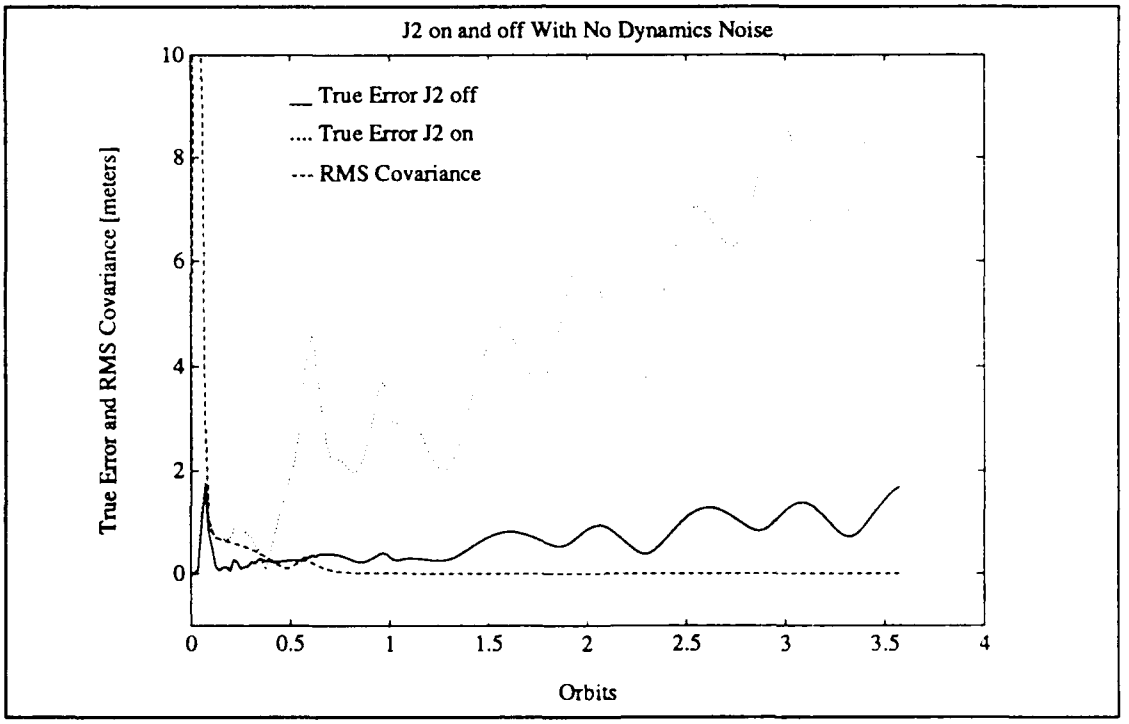

Figure 9. True error and rms covariance for J_2 *on* and *off* with no dynamics noise.

reaching *perfection*. Notice, however, that the divergence is larger in the case with J_2 on. This also is expected in light of the significant non-linearities and coupling in the equations of motion with J_2 present.

The filter was tested against the work done by Capt Johnston [7:36-37]. The J_2 term was toggled *off* in order to directly compare the results with his. The $\mathbf{P}_0$ and $\mathbf{Q}_d$ from Capt Johnston's work were used in the iterated, extended Kalman filter. Results were similar to his. After minor tuning, the iterated, extended Kalman filter yielded a true error near 8 cm, as seen in Figure 10.

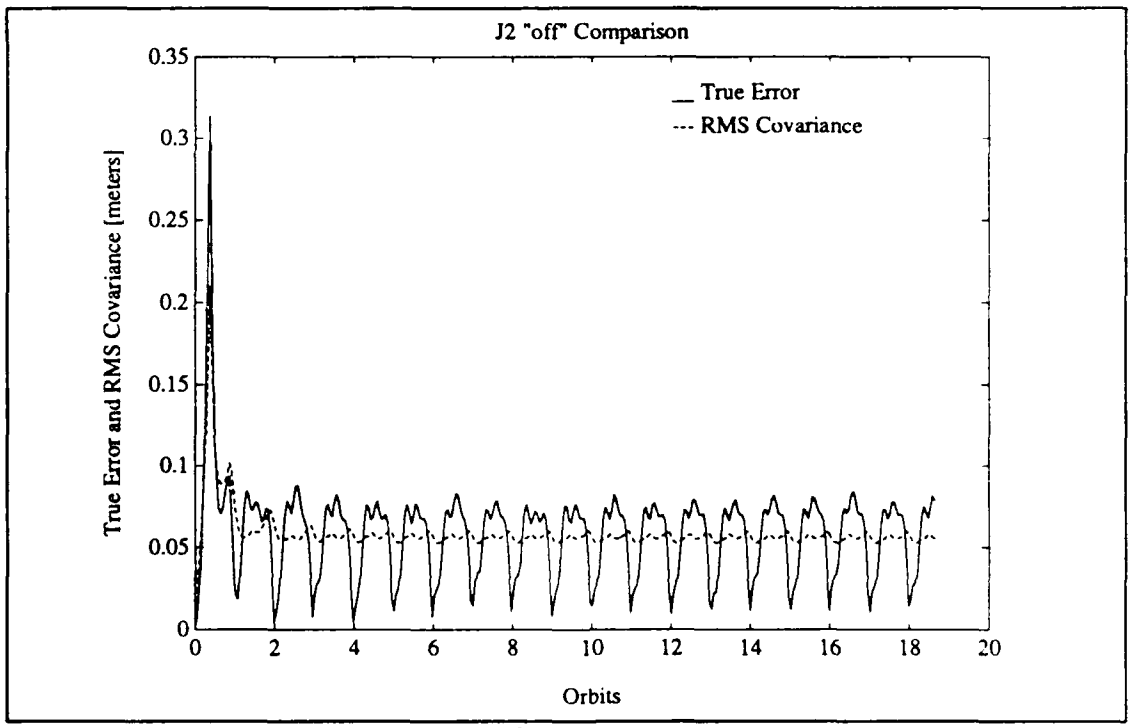

Figure 10. J_2 *off* comparison with Capt Johnston's work.

3.4 Filter Tuning Against J_2

The values of $\mathbf{Q}_d$ from the J_2 *off* case were used to serve as a starting point to tune against the truth model with J_2 *on*. The results of this are shown in Figure 11. As can be seen, more tuning is needed and there is a strong divergence near 20 orbits. After numerous attempts to adjust $\mathbf{Q}_d$ by keeping the diagonal elements for position and for velocity the same, the filter did not tune out the divergence near 20 orbits. This was investigated further. By extending to 86 orbits the true error transient at 20 orbits appeared to be the only transient. The

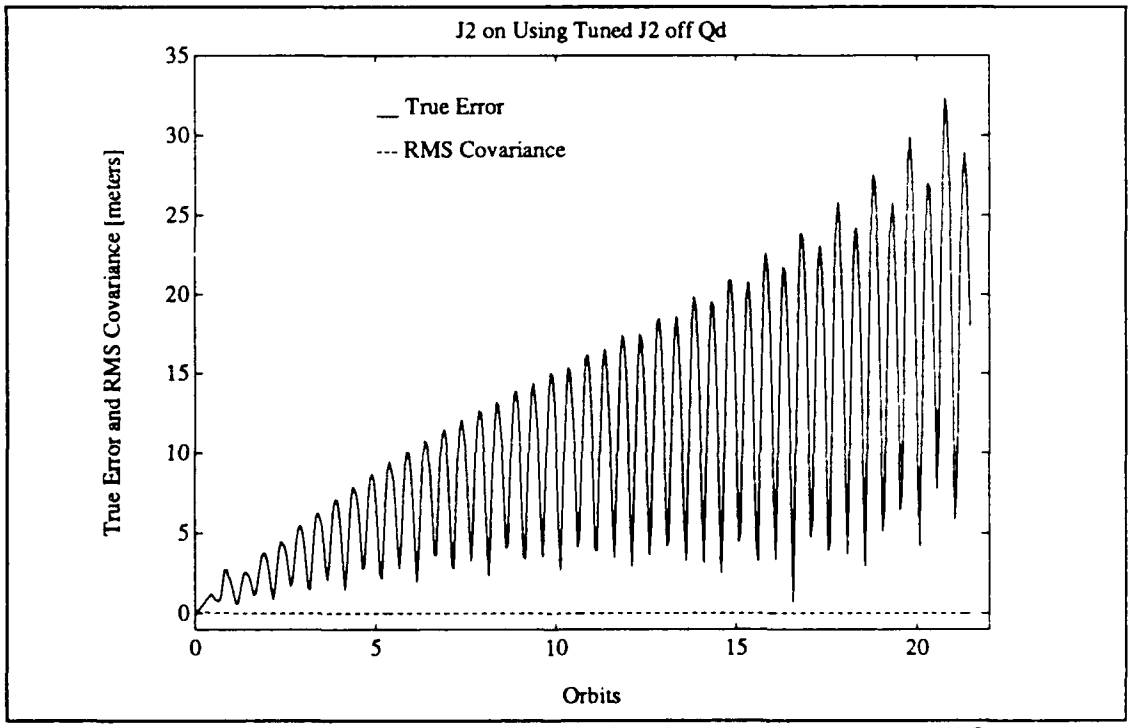

Figure 11. True error vs rms covariance for J_2 *on* using the J_2 *off* $\mathbf{Q}_d$.

behavior of the filter beyond 20 orbits was far from steady-state. The true error was diverging as can be seen in Figure 12. The transient remained after several attempts to achieve steady-state for the true error and rms covariance by adjusting the position elements and the velocity elements the same. Since the filter was running in single precision, the possibility of a numerical precision problem was investigated.

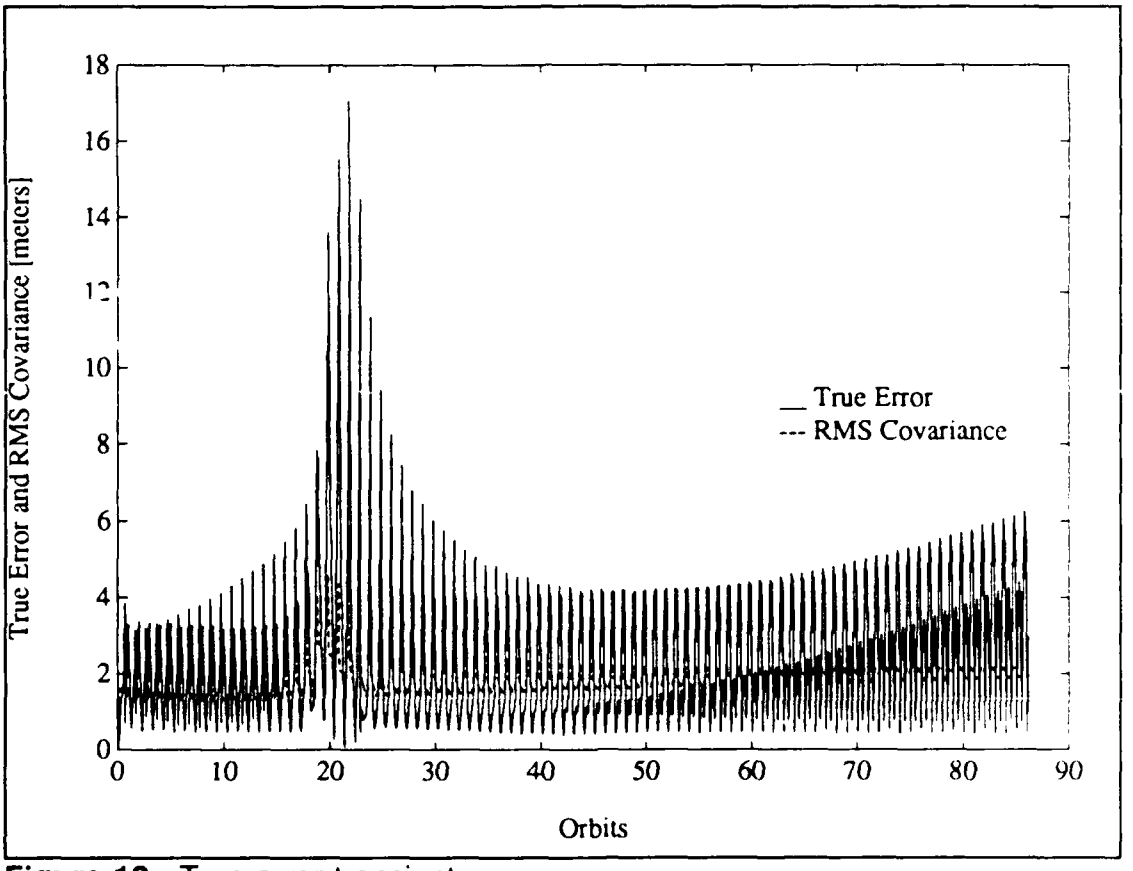

Figure 12. True error transient.

3.4.1 Numerical Precision Investigation

The filter was programmed to operate in single precision. This was done to simulate the on-board software. As a simple check, the filter was run in double precision. The filter performed the same as in single precision. Figure 13 shows the comparison for approximately 20 orbits. Further investigation into the dynamics was warranted.

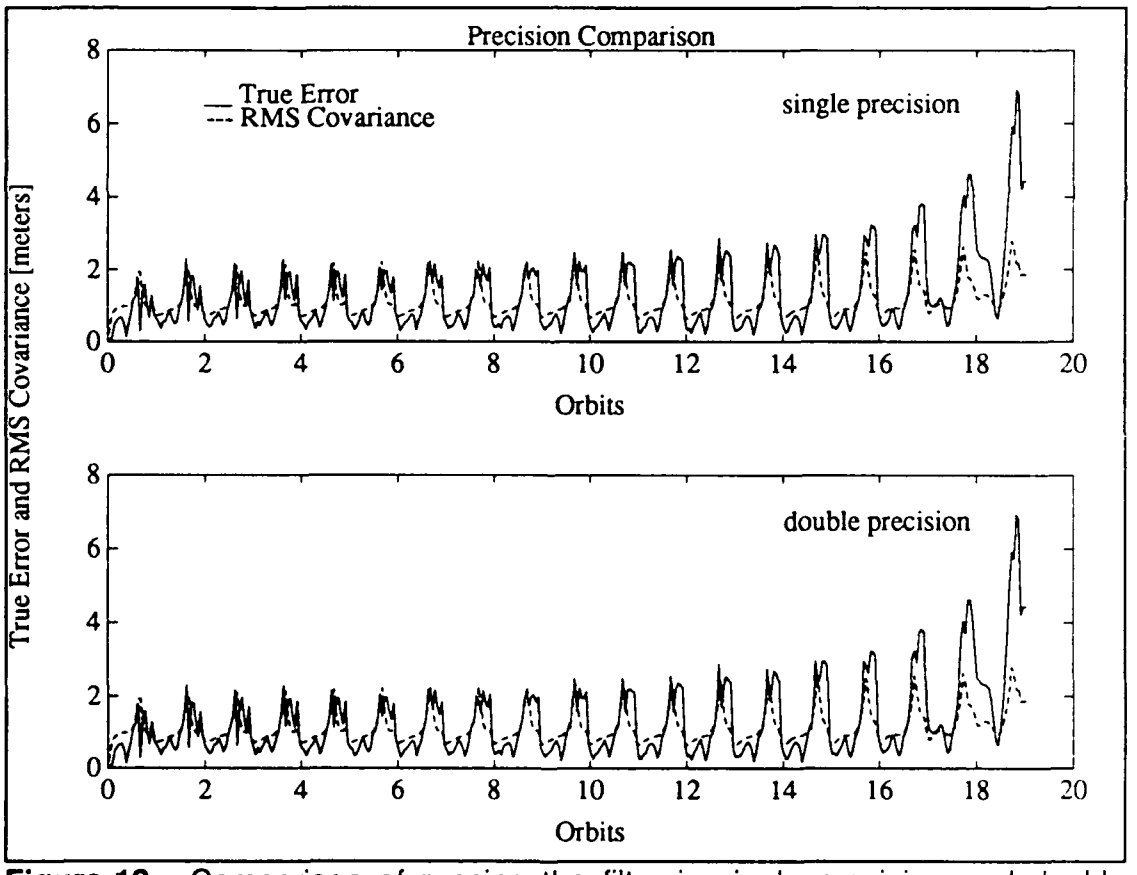

Figure 13. Comparison of running the filter in single precision and double precision.

3.4.2 Individual Component Investigation

In order to isolate the state elements that were causing this behavior, the position true error and rms covariance were plotted for each axis. Figure 14 indicates the y and z components as having the most error accounting for the transient and divergence. The Clohessy-Wiltshire equations uncouple the z position and velocity components, and do not account for the drift in the relative orbits. This is consistent with the actual relative orbits depicted in Figure 5. Following this, all six position and velocity elements were then adjusted individually.

The uncertainty in the dynamics is attributed to an uncertainty in the accelerations due to J_2. These are represented by velocity elements in $\mathbf{Q}_d$. To get a handle on these elements, an acceleration based on the amount of drift in each direction was found. From these accelerations, the elements of $\mathbf{Q}_d$ were obtained.

Appropriate values for the accelerations were obtained from the distance the vehicles have drifted in each direction per orbit,

$$d_{drift} = \frac{1}{2} a_{drift} t^2 \qquad (57)$$

where appropriate values for d_{drift} were obtained from Figure 5, and t is the orbital period of approximately 6300 seconds. Using a $d_{drift,y}$ of 20 m (200 m/10 orbits), $a_{drift,y}$ is approximately 1×10^{-6} m/s^2. Similarly, for $d_{drift,z}$ of 5 m, $a_{drift,z}$ is 2.5×10^{-7}

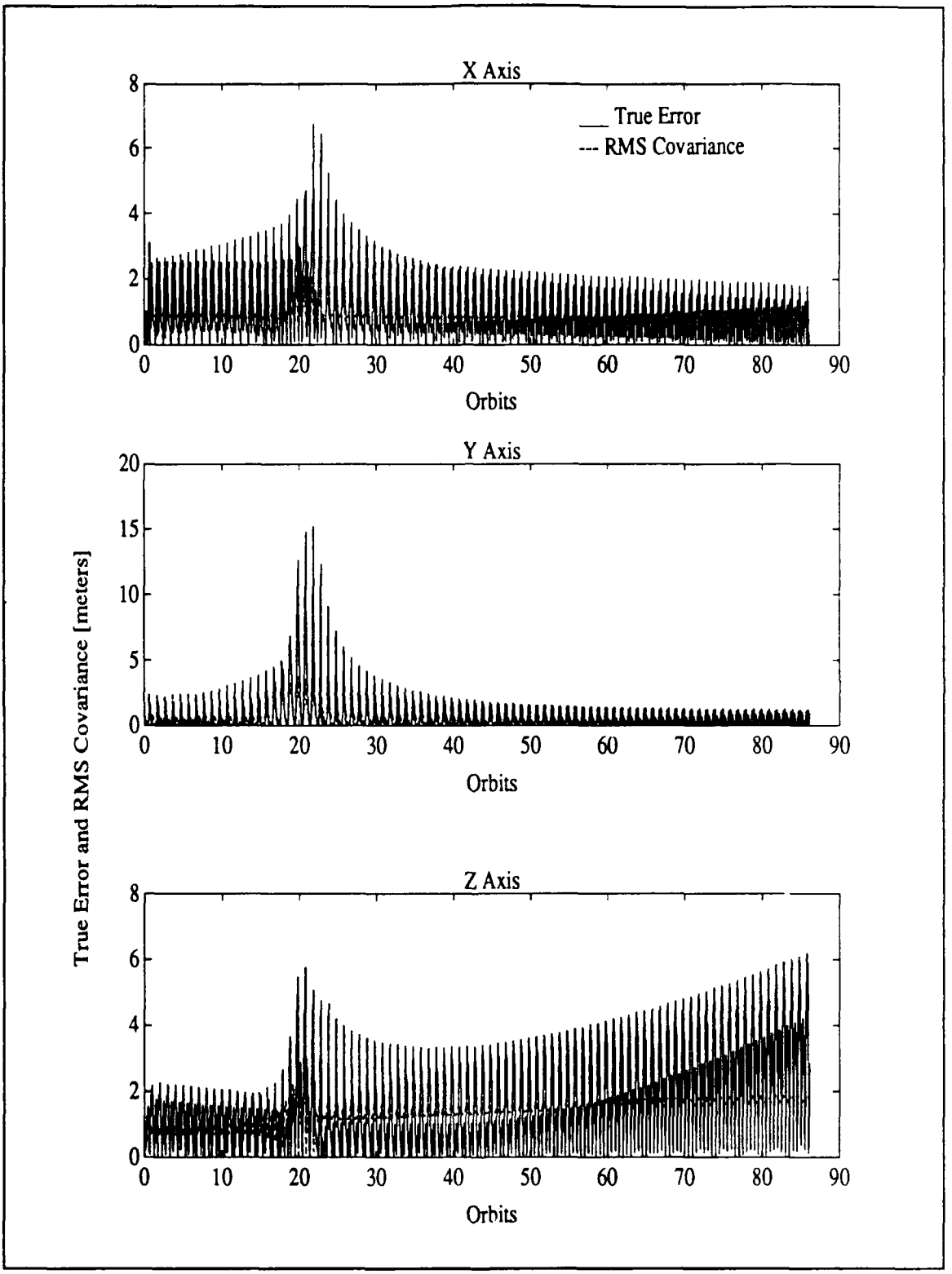

Figure 14. Component breakout of true error and rms covariance.

m/s^2. The x component shows little drift, and therefore $a_{drift,x}$ will be based on a $d_{drift,x}$ equal to the range measurement error assumed, (.01 m). This equates to an $a_{drift,x}$ of 5×10^{-10} m/s^2.

Using these accelerations, better estimates of the velocity elements of $\mathbf{Q}_d$ were found by

$$\mathbf{Q}_{d,v_x,v_y,v_z} = (a_{drift,x,y,z}\Delta t)^2 \tag{58}$$

Using an update rate of 300 seconds yields v_x, v_y, and v_z elements of 2.25×10^{-14} m^2/s^2, 9×10^{-8} m^2/s^2, and 5.6×10^{-9} m^2/s^2 respectively. By using Eq (57) with $t = \Delta t$ a better estimate of the position elements of $\mathbf{Q}_d$ were found. Using the update rate of 300 seconds gives the x, y, and z elements of 2.25×10^{-5} m^2, 4.5×10^{-2} m^2, and 1.1×10^{-2} respectively. The results using these values are shown in Figure 15.

3.4.3 Utilizing the Kozai Mean Motion

Even with these values for $\mathbf{Q}_d$, the filter still was not tuning out the transient. The dynamics model in the estimator was augmented. The Clohessy-Wiltshire equations are in the desired linear form. In order to keep the equations linear the mean motion was changed to the Kozai form.

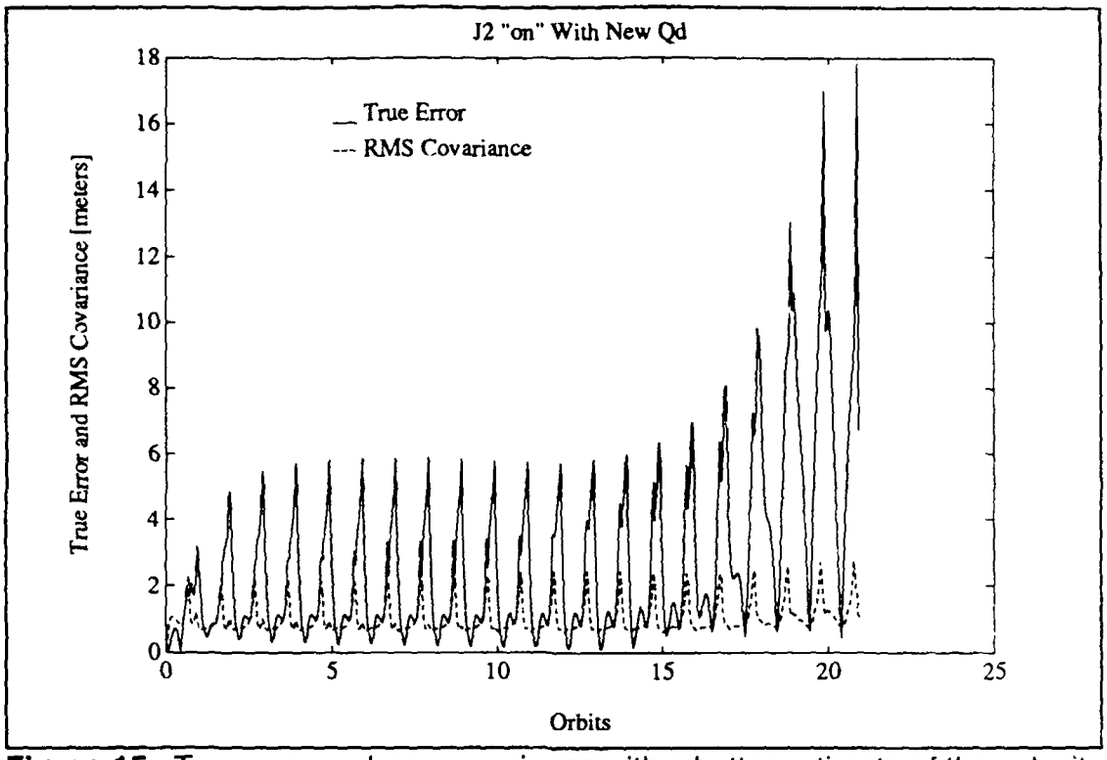

Figure 15. True error and rms covariance with a better estimate of the velocity elements of $\mathbf{Q}_d$.

The Kozai form is given by [4:369]

$$\eta_K = \eta\left[1 + \frac{3}{2}\frac{J_2}{a^2(1 - e^2)^{1/2}}\left(1 - \frac{3}{2}\sin^2 i\right)\right] \tag{59}$$

The relative orbits displayed in Figure 16 show the effect of using η_K. This approach at incorporating J_2, only improves the prediction of the drift in the y direction. It doesn't couple the equations of motion. Therefore, the y components of position and velocity will need less noise than anticipated above.

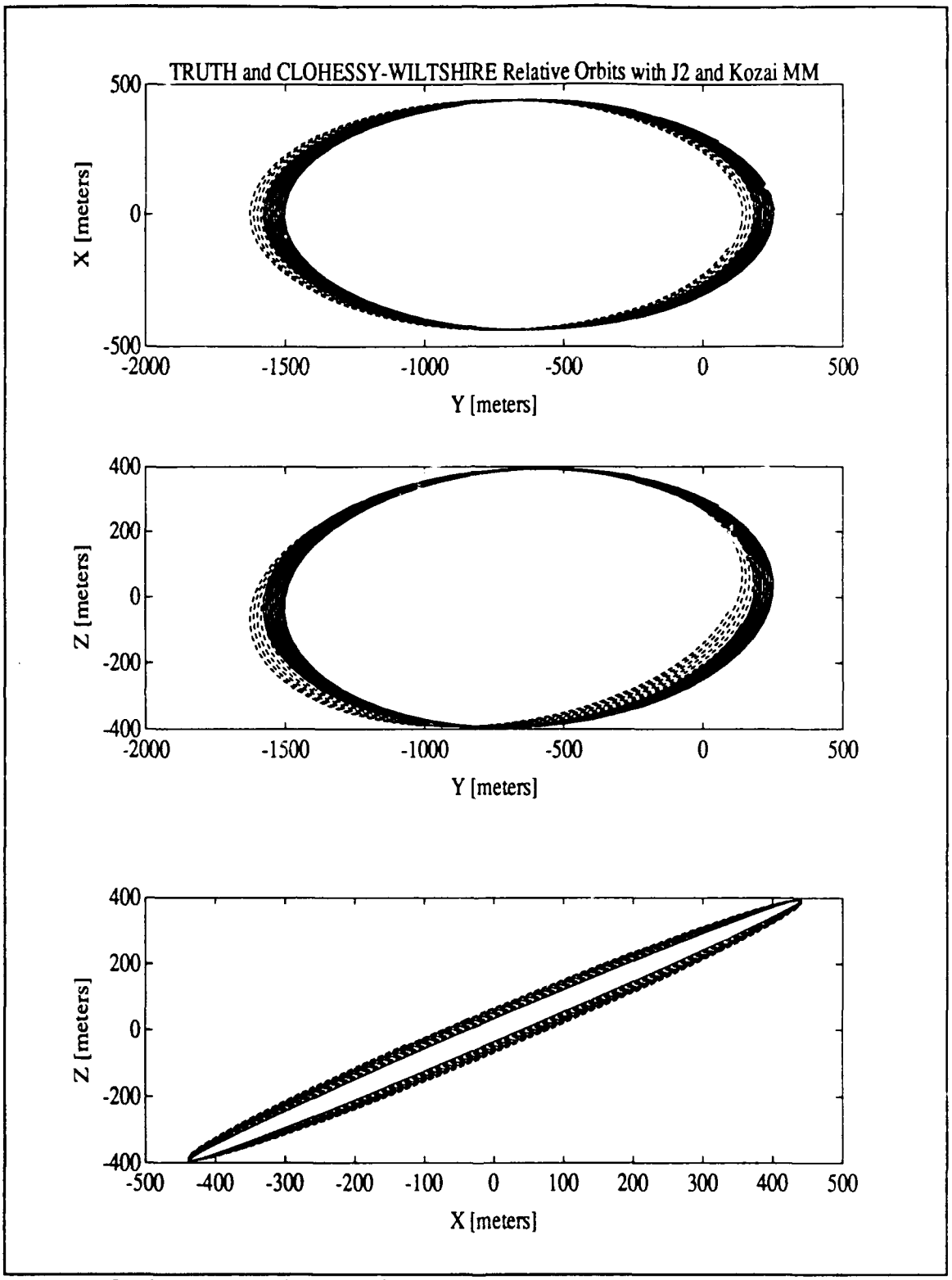

Figure 16. *Real* dynamics and Clohessy-Wiltshire equations using η_K (10 orbits).

With this in mind numerous attempts were made at tuning the filter. The filter showed results that had some sort of steady-state behavior as seen in Figure 17.

3.5 "Tuned" Performance Analysis

The filter "tuned" against J_2 did not perform as well as against the Newtonian truth model. This might be expected since the filter dynamics are a 1st order approximation of the point mass orbit, while the J_2 truth model is highly non-

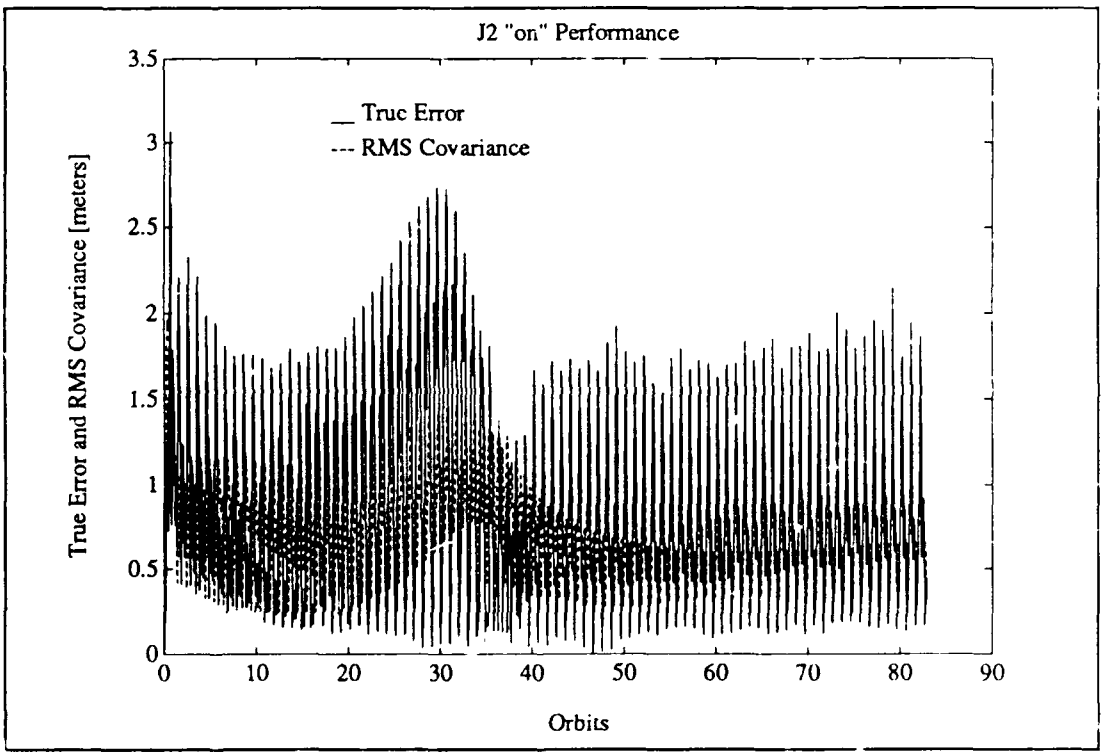

Figure 17. "Tuned" filter performance.

linear and coupled with a perturbing acceleration. "Steady-state" is seen in Figure 17 to be approximately 1 to 2 meters. Although its performance does not compare to the point mass analysis, the filter still remains within the allowed tolerance of 25 meters for the 86 orbits.

3.6 Long Term Performance

Although Figure 17 shows the true error below the 25 meter accuracy requirement for as long as 86 orbits, the behavior is questionable when compared to the J_2 *off* case. The final analysis was to determine if the filter's dynamics had sufficient fidelity to model the J_2 effects or if the iterated, extended Kalman filter was not providing adequate response. In order to assess this, both the J_2 *on* and J_2 *off* case were run for 30 days.

The filter remained "steady-state" for quite awhile before exhibiting non-steady-state behavior in the true error for the J_2 *on* case. This divergence is greater in amplitude than the previous transient at 20 orbits. Figure 18 shows the long term behavior of 30 days. The true error diverged, while the rms covariance did not converge. Figure 19 shows the J_2 *off* case run for 30 days as well.

Both cases were run using sample times varying from 112 seconds to 300 seconds in order to improve the filter's response. No significant improvements resulted; therefore, the 300 second sample time was used in order to keep

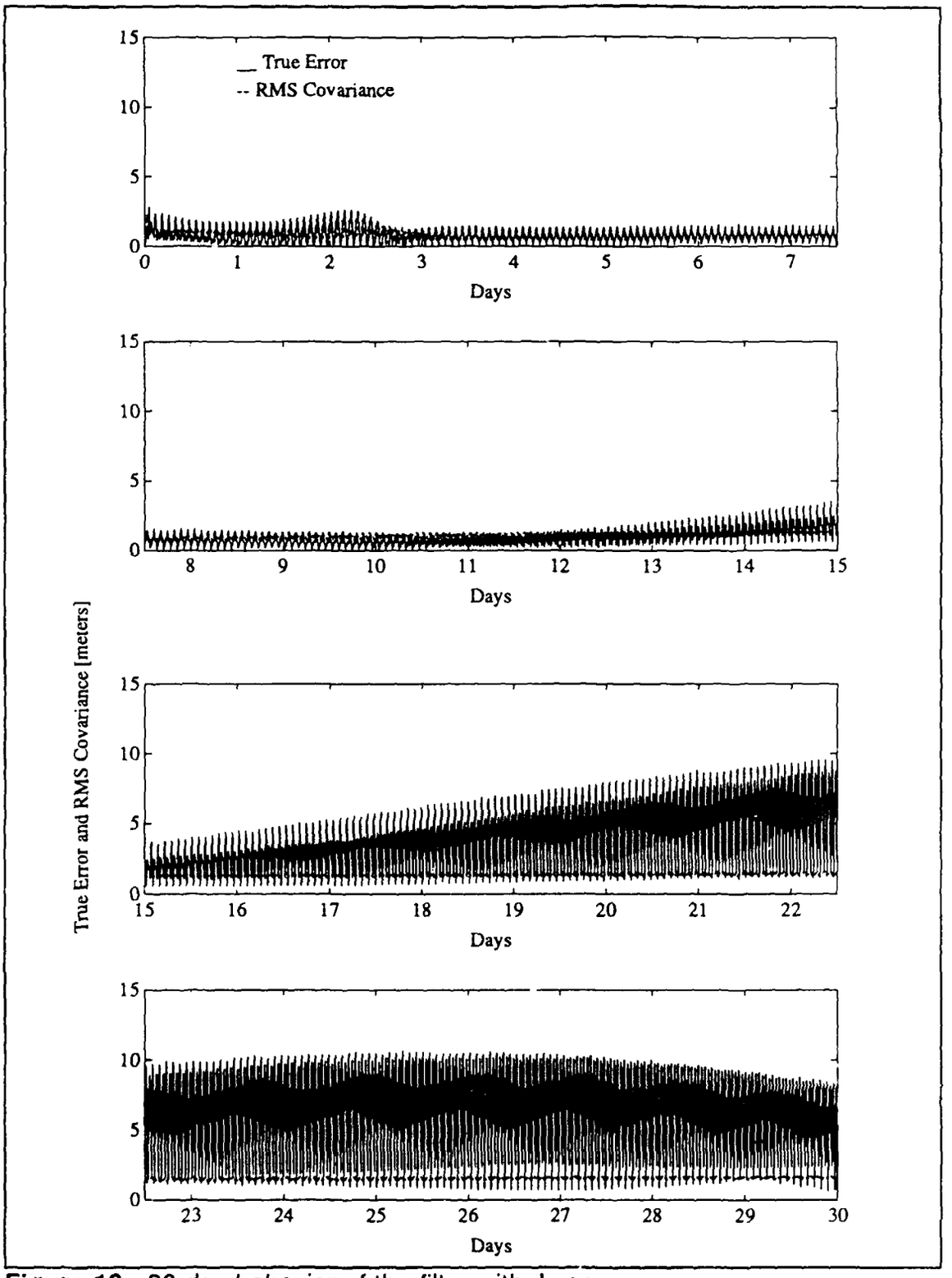

Figure 18. 30 day behavior of the filter with J_2 *on*.

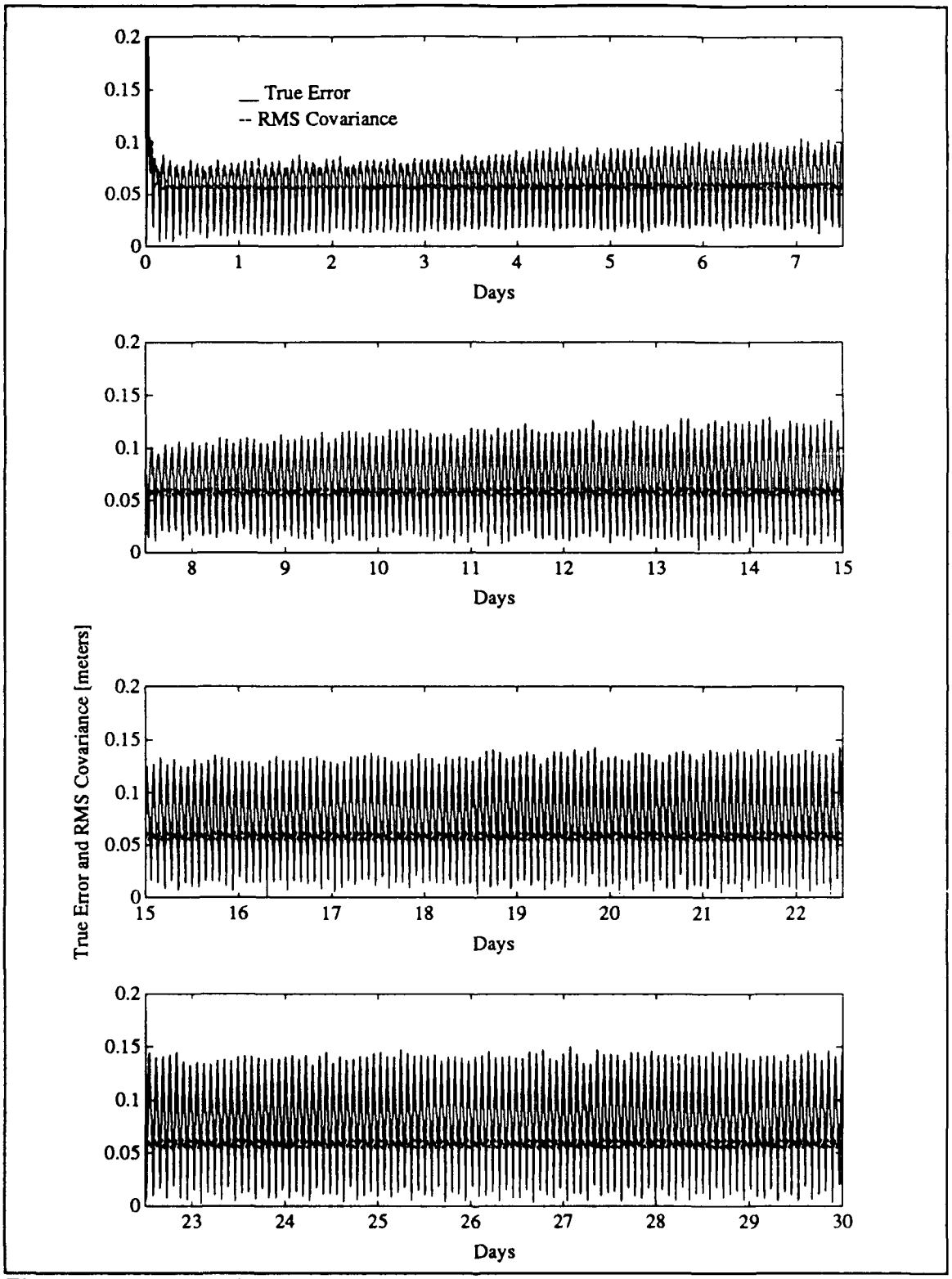

Figure 19. 30 day behavior of the filter with J_2 *off.*

computation time down.

The filter showed smooth behavior for the J_2 *off* case for the entire 30 days. This indicates the iterated, extended Kalman filter has adequate ability to handle the problem if the dynamics models are comparable. Since the performance in the J_2 *on* case is poor compared to the J_2 *off* case, it is evidence that the filter dynamics do not have adequate ability to model the truth dynamics.

IV. Conclusions and Recommendations

The use of the iterated, extended Kalman filter yielded satisfactory results for the J_2 *off* case, given the accuracy requirements. However, the analysis presented here indicates the performance is poor for the filter dynamics model when run against the J_2 *on* case. This indicates the filter dynamics need to be modified more substantially than was done. The Clohessy-Wiltshire equations had good performance against the Newtonian point mass dynamics, due to the fact they are the first order form of the point mass dynamics. Any update in the filter was readily propagated forward to first order accuracy. This is a significant factor of the filter's performance.

However, only the range was used as data, and therefore only partially modified the position and velocity elements of the state, given the observation relationships, Eqs (41) and (44). Against the Newtonian point mass dynamics, the velocity elements did not necessarily need to be updated with data since the dynamics already had good fidelity of the *truth* dynamics. In contrast, against the J_2 *truth* dynamics, the fidelity of the Clohessy-Wiltshire equations was poor, as seen in Figure 5 and Figure 16. This is primarily due to the uncoupling of the z components and the exclusion of J_2 effects.

Although the Clohessy-Wiltshire equations are valid for any down range relative position, they are valid only for small relative positions in the radial and

out-of-plane components [13;80], and hence only small periods of time. The filter uses the Clohessy-Wiltshire trajectory only for a small period of time, the sample period. In this sample period the state changes only by a small amount. Therefore, the dynamics may give sufficient performance for the sample period, but the state not being fully updated may prevent adequate performance against J_2 *on*. The significant amount of tuning by adjusting diagonal elements of $\mathbf{Q}_d$ tried to overcome these problems.

Improved performance should be obtainable by either improving the filter dynamics or by including range rate in the filter's observation relationships. The first assumes a linear form of relative motion equations to include J_2 effects, eccentricity and coupling of the equations of motion. The second assumes the satellite's ability to sense range rate. However, this may complicate the satellite's hardware design too much, negating the idea to keep the satellites as simple as possible.

Further work should include a better filter dynamics model such as referenced in [6]. Alternately, both range and range rate observation relationships should be used. Having established the new dynamic or observation relations, a complete Monte-Carlo analysis should be run. Since the filter is required to perform for several satellites, it should be run against several initial conditions to evaluate its robustness.

```
      SUBROUTINE HAMING(NXT)

* Version of 11/07/90
* Purpose
*    Subroutine for integrating a system of first order differential
*    equations.  It is a fourth order predictor-corrector algorithm
*    which means it carries the last four values of the state vector,
*    and extrapolates these values to obtain a predicted next value
*    (the prediction step) and evaluates the equations of motion at
*    the predicted point, and then corrects the extrapolated point
*    using a higher order polynomial (the correction step).
* Input
*    NXT = specifies which of the four values of the state vector is
*          the current one.  NXT is updated by HAMING automatically,
*          but must be set to ZERO on the first call.
* Call Subroutines
*    RHS(NXT) = evaluates the equations of motion
* External Functions
*    None
* Common Blocks
*    HAM = Memory block shared by the main driver and subroutine RHS.
*    The common block contains:
*      X       = is the independent variable (often time)
*      Y(MAX,4) = the state vector (4 copies), with NXT pointing to
*               the current one, the limit of MAX EOM can be changed
*               through the PARAMETER in main driver, sub program
*               RHS, and below.
*      F(MAX,4) = are the EOM evaluated at the same times as the state
*               vector Y ... it is the job of sub program RHS to
*               calculate these.
*      ERR(MAX) = is an estimate of the one-step integration error
*      N       = is the number of ODES ... limit is MAX unless you change
*               the PARAMETER statement in main driver, sub program
*               RHS, and below.
*      H       = is the timestep ... one call to HAMING increments X by H
* References
*    "Numerical Methods for Scientists and Engineers", Richard W. Hamming;
```

```
*      McGraw- Hill, 2nd Ed., 1973; pp. 361-408
*
*      Donald G. M. Anderson -- Harvard (1972)
*     Original program modified by Dr. William E. Wiesel and Dr. Rodney Bain.
* Comments
*     TOL = is HAMING's startup tolerance ... set to reasonable value
*           as necessary in PARAMETER statement.
*     The user must supply a main driver, and the subroutine RHS(NXT)
*     which evaluates the equations of motion.

      IMPLICIT REAL*8 (A-H,O-Z)    ! Global double precision
      PARAMETER (ZERO=0.D0, ONE=1.D0, TWO=2.D0, THREE=3.D0,
     1           FOUR=4.D0, MAX=42, TOL=1.D-12)
      COMMON /HAM/ X,Y(MAX,4),F(MAX,4),ERR(MAX),N,H

* Check if this is the first call ... HAMING (like all predictor-
* correctors) needs 'previous' values

      IF(NXT) 190,10,200

* It is a forward Picard iteration (slow and expensive) to step
* backwards in time three steps to get the 4 previous points.  A
* successful startup returns NXT=1, and time has not been
* incremented.  If startup fails, NXT will be returned as ZERO.

 10   XO=X
      HH=H/TWO
      CALL RHS(1)
      DO 40 L=2,4
        X=X+HH
          DO 20 I=1,N
 20         Y(I,L)=Y(I,L-1)+HH*F(I,L-1)
        CALL RHS(L)
        X=X+HH
          DO 30 I=1,N
 30         Y(I,L)=Y(I,L-1)+H*F(I,L)
 40     CALL RHS(L)
      JSW=-10
 50   ISW=1
      DO 120 I=1,N
        HH=Y(I,1)+H*(9.D0*F(I,1)+19.D0*F(I,2)-5.D0*F(I,3)
```

```
     1      +F(I,4))/24.D0
            IF( DABS(HH-Y(I,2)) .LT. TOL) GOTO 70
            ISW=0
 70         Y(I,2)=HH
            HH=Y(I,1)+H*(F(I,1)+FOUR*F(I,2)+F(I,3))/THREE
            IF( DABS(HH-Y(I,3)) .LT. TOL) GOTO 90
            ISW=0
 90         Y(I,3)=HH
            HH=Y(I,1)+H*(THREE*F(I,1)+9.D0*F(I,2)+9.D0*F(I,3)
           1   +THREE*F(I,4))/8.D0
            IF( DABS(HH-Y(I,4)) .LT. TOL) GOTO 110
            ISW=0
110         Y(I,4)=HH
120         CONTINUE
            X=XO
            DO 130 L=2,4
              X=X+H
130           CALL RHS(L)
            IF(ISW) 140,140,150
140         JSW=JSW+1
            IF(JSW) 50,280,280
150         X=XO
            ISW=1
            JSW=1
            DO 160 I=1,N
160           ERR(I)=ZERO
            NXT=1
            GOTO 280

*  A call to HAMING with NXT=-NXT, after a successful startup,
*  will turn off the second evaluation of the equations of motion
*  following the corrector step.  In systems where the equations of
*  motion are very expensive, this can halve your run time.

190         JSW=2
            NXT=IABS(NXT)

*  This is the predictor-corrector algorithm ... first the indices
*  are premuted.

200         X=X+H
```

```
      NP1=MOD(NXT,4)+1
      GOTO (210,230),ISW
  210 GOTO (270,270,270,220),NXT
  220 ISW=2
  230 NM2=MOD(NP1,4)+1
      NM1=MOD(NM2,4)+1
      NPO=MOD(NM1,4)+1

*  ... then the predictor part is run to find an extrapolated value
*  of the state vector at the new time ...

      DO 240 I=1,N
        F(I,NM2)=Y(I,NP1)+FOUR*H*(TWO*F(I,NPO)-F(I,NM1)
     1          +TWO*F(I,NM2))/THREE
  240   Y(I,NP1)=F(I,NM2)-0.925619835D0*ERR(I)

*  The equations of motion are evaluated at the extrapolated value
*  of the state vector ...

      CALL RHS(NP1)

*  and the corrector algorithm is used to add this new information
*  and obtain a better value of the new state vector ...

      DO 250 I=1,N
        Y(I,NP1)=(9.D0*Y(I,NPO)-Y(I,NM2)+THREE*H*(F(I,NP1)
     1          +TWO*F(I,NPO)-F(I,NM1)))/8.D0
        ERR(I)=F(I,NM2)-Y(I,NP1)
  250   Y(I,NP1)=Y(I,NP1)+0.0743801653D0*ERR(I)
      GOTO (260,270),JSW

*  Finally, the equations of motion are re-evaluated at the better
*  value of the state vector ... this can be suppressed.

  260 CALL RHS(NP1)
  270 NXT=NP1

  280 RETURN
      END
```

Bibliography

1. Bate, Roger, Donald D. Mueller, and Jerry E. White. *Fundamentals of Astrodynamics*. New York: Dover Publications, 1971.

2. Boden, Daryl G. and Bruce A. Conway. "A Comparison of Nonlinear Filters for Orbit Determination", *Astrodynamics Conference, AIAA Paper 86-2055*. Williamsburg, VA: American Institute of Aeronautics and Astronautics, August 1986.

3. Dunning, Robert Scott. "The Orbital Mechanics of Flight Mechanics". *NASA SP-325*. National Aeronautics and Space Administration, 1973.

4. Escobal, Pedro R. *Methods of Orbit Determination*. John Wiley and Sons, Inc., 1965.

5. Filer, Captain Sherrie Norton. *Investigation of the Observability of a Satellite Cluster in a Near Circular Orbit*. MS Thesis, AFIT/GA/ENY/89D-2, School of Engineering, Air Force Institute of Technology (AU), Wright-Patterson AFB OH, December 1989.

6. Hujsak, R. S. "A Non-linear Dynamical Model of Relative Motion for the Orbiting Debris Problem." *Astrodynamics 1989: Proceedings of the AAS/AIAA Astrodynamics Conference (AAS/AIAA Paper 89-397)*. American Astronautical Society, San Diego CA, 1989.

7. Johnston, Captain Stephen C. *Autonomous Navigation of a Satellite Cluster*. MS Thesis, AFIT/GA/ENY/90D-9, School of Engineering, Air Force Institute of Technology (AU), Wright-Patterson AFB OH, December 1990.

8. Maybeck, Peter S. *Stochastic Models, Estimation, and Control Volume 1*. New York: Academic Press, 1979.

9. Maybeck, Peter S. Stochastic Models, *Estimation, and Control Volume 2*. New York: Academic Press, 1982.

10. Ward, Captain Michael L. P. *Estimated Satellite Cluster Elements in Near Circular Orbit*. MS Thesis, AFIT/GA/AA/88D-13, School of Engineering, Air Force Institute of Technology (AU), Wright-Patterson AFB OH, December 1988.

11. Wiesel, William E. Class text distributed in MECH 731, *Modern Methods of Orbit Determination*. School of Engineering, Air Force Institute of Technology (AU), Wright-Patterson AFB OH, April 1990.

12. Wiesel, William E. Class text distributed in MECH 636, *Advanced Astrodynamics*. School of Engineering, Air Force Institute of Technology (AU), Wright-Patterson AFB OH, January 1991.

13. Wiesel, William E. *Spaceflight Dynamics*. New York: McGraw-Hill, 1989.

REPORT DOCUMENTATION PAGE

Form Approved
OMB No 0704-0188

1. AGENCY USE ONLY (Leave blank)	2. REPORT DATE	3. REPORT TYPE AND DATES COVERED
	December 1991	Master's Thesis

4. TITLE AND SUBTITLE
NAVIGATION OF A SATELLITE CLUSTER WITH REALISTIC DYNAMICS

5. FUNDING NUMBERS

6. AUTHOR(S)
J. Timothy Middendorf

7. PERFORMING ORGANIZATION NAME(S) AND ADDRESS(ES)
Air Force Institute of Technology
WPAFB, OH 45433-6583

8. PERFORMING ORGANIZATION REPORT NUMBER
AFIT/GA/ENY/91D-5

9. SPONSORING MONITORING AGENCY NAME(S) AND ADDRESS(ES)

10. SPONSORING MONITORING AGENCY REPORT NUMBER

11. SUPPLEMENTARY NOTES

12a. DISTRIBUTION/AVAILABILITY STATEMENT
Approved for public release; distribution unlimited

12b. DISTRIBUTION CODE

13. ABSTRACT (Maximum 200 words)

Previous work in the area of estimation of relative positions within a satellite cluster showed favorable results. However, the work was done using point mass orbits in the truth model. This thesis investigates the estimation of relative satellite positions operating in near circular orbits including the J_2 term in Earth's geopotential. The iterated, extended Kalman filter is used as the on-board estimator in order to gain better performance in the face of the non-linearities. The dynamics in the estimator are based on the Clohessy-Wiltshire equations for relative orbital motion. Inputs to the host estimator are range measurements from each satellite in the cluster. The relative position to the host satellite is investigated. A comparison of the true error and the root mean square covariance was performed..

14. SUBJECT TERMS
Satellite Cluster Kalman Filter Clohessy-Wiltshire

15. NUMBER OF PAGES
67

16. PRICE CODE

17. SECURITY CLASSIFICATION OF REPORT	18. SECURITY CLASSIFICATION OF THIS PAGE	19. SECURITY CLASSIFICATION OF ABSTRACT	20. LIMITATION OF ABSTRACT
Unclassified	Unclassified	Unclassified	UL